Fully Constrained Least Squares Linear Spectral Mixture Analysis Method for Material Quantification in Hyperspectral Imagery

Daniel C. Heinz, *Student Member, IEEE,* and Chein-I Chang, *Senior Member, IEEE*

***Abstract*—Linear spectral mixture analysis (LSMA) is a widely used technique in remote sensing to estimate abundance fractions of materials present in an image pixel. In order for an LSMA-based estimator to produce accurate amounts of material abundance, it generally requires two constraints imposed on the linear mixture model used in LSMA, which are the abundance sum-to-one constraint and the abundance nonnegativity constraint. The first constraint requires the sum of the abundance fractions of materials present in an image pixel to be one and the second imposes a constraint that these abundance fractions be nonnegative. While the first constraint is easy to deal with, the second constraint is difficult to implement since it results in a set of inequalities and can only be solved by numerical methods. Consequently, most LSMA-based methods are unconstrained and produce solutions that do not necessarily reflect the true abundance fractions of materials. In this case, they can only be used for the purposes of material detection, discrimination, and classification, but not for material quantification. In this paper, we present a fully constrained least squares (FCLS) linear spectral mixture analysis method for material quantification. Since no closed form can be derived for this method, an efficient algorithm is developed to yield optimal solutions. In order to further apply the designed algorithm to unknown image scenes, an unsupervised least squares error (LSE)-based method is also proposed to extend the FCLS method in an unsupervised manner. A series of computer simulations and real hyperspectral data experiments were conducted to demonstrate the performance of the proposed FCLS LSMA approach in material quantification.**

***Index Terms*—Fully constrained least squares (FCLS), linear spectral mixture analysis (LSMA), nonnegatively constrained least squares (NCLS), sum-to-one constrained least squares (SCLS), unsupervised FCLS (UFCLS).**

NOMENCLATURE

ANC	abundance nonnegativity constraint;
ASC	abundance sum-to-one constraint;
AVIRIS	airborne visible/infrared imaging spectrometer;
FCLS	fully constrained least squares;
HYDICE	hyperspectral digital imagery collection experiment;
LSE	least squares error;
LSMA	linear spectral mixture analysis;
LS	least squares;
NCLS	nonnegatively constrained least squares;
NNCLS	normalized NCLS;
NSCLS	normalized SCLS;
OSP	orthogonal subspace projection;
SCLS	sum-to-one constrained least squares;
UFCLS	unsupervised FCLS.

Manuscript received December 14, 1999; revised May 30, 2000. This work was supported by the Bechtel Nevada Corporation under Contract DE-AC08-96NV11718 through the Department of Energy, Washington, DC.

The authors are with the Remote Sensing Signal and Image Processing Laboratory, Department of Computer Science and Electrical Engineering, University of Maryland-Baltimore County, Baltimore, MD 21250 USA (e-mail: cchang@umbc.edu).

Publisher Item Identifier S 0196-2892(01)02086-1.

I. INTRODUCTION

SPECTRAL mixture analysis has been widely used in remote sensing for versatile applications such as material discrimination, detection, and classification. A wealth of spectral mixture analysis techniques have been reported in the literature [1]–[12]. In multispectral/hyperspectral imagery, a pixel is generally mixed by a number of materials present in the scene. Two models have been proposed in the past to describe such mixing activities. One is the macroscopic mixture [11], which models a mixed pixel as a linear combination of materials with relative concentrations. A second model suggested by Hapke in [12], called the intimate spectral mixture, is a nonlinear mixing of materials. Nevertheless, Hapke's model can be linearized by a method proposed by Johnson *et al.* [13]. Consequently, only linear spectral mixture analysis (LSMA) will be considered in this paper. By taking advantage of the linear mixture model, many image processing techniques can be applied. However, there is a principal difference between pure and mixed pixel processing, where the former is a spatial analysis technique and the latter is a spectral analysis technique. For example, mixed pixel classification attempts to estimate the abundance fractions of materials of interest in a pixel and classifies these materials in accordance with their estimated abundance fractions as opposed to standard class membership assignment-based pure pixel classification. As a result, the mixed pixel classification generally generates a gray scale image whose gray level values are determined by the estimated abundance fractions of the materials resident in the image pixels in contrast to the class-designated images produced by the pure pixel classification.

LSMA-based methods require *a priori* knowledge of the signatures of materials present in the image scene, which is generally not available. Under this circumstance, selection of an appropriate set of material signatures is crucial for successful performance of any LSMA-based method. In the ideal case, these signatures would represent pure spectral signatures of all materials in the image scene. Unfortunately, this case is rarely true in practical situations since all the signatures to be used are generally obtained directly from the image scene, in either a supervised or an unsupervised fashion. Suppose that

$\mathbf{m}_1, \mathbf{m}_2, \cdots, \mathbf{m}_p$ are the signatures of materials resident in an image scene, and $\alpha_1, \alpha_2, \cdots, \alpha_p$ are their associated abundance fractions. It should be noted that an image pixel does not necessarily contain all the p material signatures For instance, when some signature, say$\mathbf{m}_j$, is absent from the pixel, its corresponding abundance α_j will be zero, $\alpha_j = 0$. This implies that an image scene may contain as many as p materials, while a pixel may contain only one or a few materials. In order for an LSMA-based method to provide accurate and reliable estimates of signature abundance fractions for material quantification, two constraints must be imposed on the abundance fractions of materials in a pixel: 1) abundance sum-to-one constraint (ASC) $\sum_{j=1}^{p} \alpha_j = 1$ and 2) abundance nonnegativity constraint (ANC) $\alpha_j \geq 0$ for all $1 \leq j \leq p$. A fully constrained LSMA method will simultaneously implement the ASC and the ANC. While the ASC is easy to deal with, the ANC is difficult to implement in practice, since the ANC results in a set of inequalities and cannot be solved analytically. In this case, it must rely on numerical methods to yield optimal solutions. Due to such mathematical intractability, many LSMA-based methods are unconstrained and can only produce suboptimal solutions, e.g., minimum distance [14]–[16], singular value decomposition [17], maximum likelihood estimation (MLE) [18], [19], least squares method (LSM) [20], [21], subspace projection approaches [21]–[24], etc. Furthermore, the abundance fractions $\alpha_1, \alpha_2, \cdots, \alpha_p$ estimated by the unconstrained LSMA do not generally reflect the true and accurate abundance fractions. As a result, they cannot be used for material quantification.

In past years, some efforts were devoted to solving fully constrained linear mixing problems. However, the approaches used to implement these constraints were designed mainly for a small number of material signatures. For instance, in [20], Shimabukuro and Smith considered several constrained least squares mixing models and obtained constrained least squares solutions by solving an overdetermined system that consisted of m equations with n unknowns with $n < m$, where m is the number of bands and n is the number of signatures. Since there are no closed-form solutions, one must examine possible solutions in a feasible region bounded by the ASC and ANC. The use of quadratic programming techniques to impose the ASC and ANC were investigated in [25]–[27], but the algorithms used were computationally expensive. Another method presented in [28] also suffered from excessive computational complexity as the number of materials increases.

In this paper, we consider fully constrained linear mixing problems in hyperspectral imagery and develop a least squares-based approach to unmixing materials for quantification. Since there are no analytical solutions, an efficient numerical algorithm is further designed to generate optimal solutions. The proposed method is based on the least squares approach [29] as well as the concept of orthogonal subspace projection (OSP) developed in [22]. It first considers partially constrained least squares LSMA and then takes advantage of its solutions to solve for fully constrained linear mixing problems. Two partially constrained least squares approaches are our interest, referred to as sum-to-one constrained least squares (SCLS) and nonnegatively constrained least squares (NCLS) methods. While the SCLS method imposes only the ASC, the NCLS only requires the ANC to be imposed. The advantage of the SCLS method is that its solution can be obtained by an LSM and can be further expressed by an unconstrained least squares solution plus an error correction term. The unconstrained least squares solution in the SCLS method is identical to the least squares orthogonal subspace projection classifier derived in [23] or signature subspace classifier in [21]. In contrast, the NCLS method does not yield closed-form solutions. Nevertheless, the NCLS algorithm developed in [30] can be used to generate its solutions. The algorithm utilizes a steering matrix to iteratively force material signatures with negative abundance fractions to zero until an optimal least squares solution is obtained. By implementing this NCLS algorithm in conjunction with the ASC, an efficient algorithm, called the fully constrained least squares (FCLS) algorithm, can be developed to solve for fully constrained linear mixing problems. It is also a quadratic programming technique. However, it uses a more computationally efficient algorithm for simultaneously implementing both the ASC and ANC. The significant savings in computational cost becomes more evident when the FCLS method is extended to an unsupervised FCLS. In order to better compare the SCLS method and NCLS method against the proposed FCLS method in terms of material quantification, a normalized SCLS (NSCLS) method and normalized NCLS (NNCLS) method are also included. The NSCLS method is the same approach presented in [27] that set to zero all negative abundance estimates and rescaled the remaining abundance estimates so that they summed to one. The NNCLS method simply rescales the NCLS-estimated abundance fractions to sum to one.

One common drawback of LSMA methods is the requirement of the complete prior knowledge of material signatures present in an image scene. Unfortunately, finding such information is generally difficult. This is particularly true for hyperspectral imagery. For example, the hyperspectral digital imagery collection experiment (HYDICE) sensor has significantly improved spectral resolution of 10 nm and spatial resolution from 1–4 m when compared to multispectral sensors. With such fine spatial and spectral resolutions, the HYDICE sensor can detect targets with size as small as 1–4 m for the purpose of target detection, discrimination, classification, and identification. However, the HYDICE sensor may also extract many unknown signal sources or materials in an image scene. Obtaining prior knowledge of all material sources is a serious issue for LSMA-based methods. In order to resolve this problem, an unsupervised constrained least squares error (LSE)-based approach is further proposed to extend the FCLS algorithm to an unsupervised FCLS (UFCLS) algorithm so that the FCLS method can be implemented on an unknown image scene with no required prior knowledge.

The remainder of this paper is organized as follows. Section III briefly reviews the linear mixture model to be used throughout this paper. Sections IV and Section V describe unconstrained and partially constrained LSMA methods, respectively. Section VI presents the FCLS and UFCLS algorithms. Section VII conducts a series of computer simulations and hyperspectral imagery experiments to evaluate the performance of unconstrained, partially constrained, and fully constrained least squares-based methods. Finally, Section VIII concludes with some remarks.

II. Linear Mixture Model

Linear spectral mixture analysis is a widely used approach to determine and quantify materials in remotely sensed imagery. Since every pixel is acquired by spectral bands at different wavelengths, they can be represented as column vectors, and a hyperspectral image is actually an image cube. Suppose that l is the number of spectral bands. Let $\mathbf{r}$ be an $l\times 1$ column pixel vector in a multispectral or hyperspectral image where the bold face is used for vectors. Let M be an $l \times p$ material signature matrix denoted by $[\mathbf{m}_1\ \mathbf{m}_2 \cdots \mathbf{m}_p]$, where $\mathbf{m}_j$ is an $l\times 1$ column vector represented by the signature of the jth material resident in the image scene, and p is the number of materials in the image scene. Let $\alpha = (\alpha_1, \alpha_2, \cdots, \alpha_p)^T$ be a $p\times 1$ abundance column vector associated with $\mathbf{r}$, where α_j denotes the abundance fraction of the jth signature present in the pixel vector $\mathbf{r}$.A classical approach to solving mixed pixel classification problem is linear unmixing, which assumes that there are p materials in an image scene and the spectral signature of an image pixel vector $\mathbf{r}$ is linearly mixed by these p material signatures. In this case, the spectral signature of a pixel vector $\mathbf{r}$ can be represented by a linear regression model as follows:

$$\mathbf{r} = \mathbf{M}\alpha + \mathbf{n} \tag{1}$$

where $\mathbf{n}$ is noise or can be interpreted as a measurement error. Here, without confusion, the $\mathbf{r}$ will be used to represent either the pixel vector r or its spectral signature (i.e., digital numbers, [DNs]). A linear unmixing method attempts to unmix the unknown abundance fractions via an inverse of the linear mixture model specified by (1) so as to achieve the tasks of material discrimination, detection, classification, quantification, etc.

III. Unconstrained LSMA Methods: OSP Approach

The model given by (1) represents an unconstrained linear mixing problem. Many methods have been developed in the past to address this problem [1]–[11], [16]–[24]. In this section, we are particularly interested in the OSP approach in [21]–[23] that will lead to the proposed FCLS method.

A. Orthogonal Subspace Projection (OSP)

In the OSP approach, a single material signature of interest is selected from the material signature matrix $\mathbf{M}$ for classification. Without loss of generality, this desired material signature is assumed to be $\mathbf{d} = \mathbf{m}_p$, and $\mathbf{U} = [\mathbf{m}_1\ \mathbf{m}_2 \cdots \mathbf{m}_{p-1}]$ is the undesired material signature matrix made up of the remaining $p-1$ undesired material signatures in $\mathbf{M}$. Model (1) can be rewritten as

$$\mathbf{r} = \mathbf{d}\alpha_p + \mathbf{U}\gamma + \mathbf{n} \tag{2}$$

where γ is the abundance vector associated with $\mathbf{U}$. Equation (2) allows us to design an orthogonal subspace projector to annihilate $\mathbf{U}$ from $\mathbf{r}$ prior to classification which results in an orthogonal subspace projection (OSP) operator derived in [22] and given by

$$P_{\mathrm{OSP}}(\mathbf{r}) = \mathbf{d}^T P_{\mathbf{U}}^{\perp}(\mathbf{r}) \tag{3}$$

where

$$P_{\mathbf{U}}^{\perp} = \mathbf{I} - \mathbf{U}\mathbf{U}^{\#} \tag{4}$$

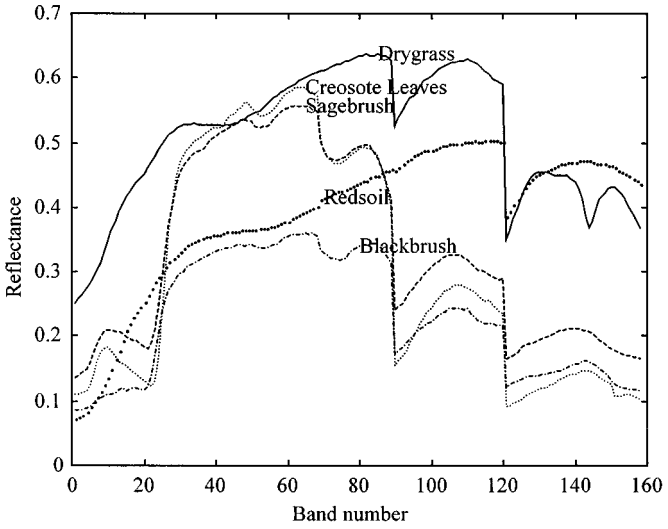

Fig. 1. Simulated AVIRIS reflectance spectra with atmospheric water bands removed.

$\mathbf{U}^{\#} = (\mathbf{U}^T\mathbf{U})^{-1}\mathbf{U}^T$ is the pseudo-inverse of U and the notation $\perp_{\mathbf{U}}$ indicates that the projector $P_{\mathbf{U}}^{\perp}$ maps $\mathbf{r}$ into the orthogonal complement of $\langle\mathbf{U}\rangle$, denoted by $\langle\mathbf{U}\rangle^{\perp}$.

B. Least Squares (LS) Projection Classifier

In the OSP classifier given by (3), the abundance vector α is assumed to be known *a priori*. In reality, α is generally not known, and needs to be estimated. In order to estimate $\alpha = (\alpha_1, \alpha_2, \cdots, \alpha_p)^T$ from the observed data, several techniques have been developed in [21], [23] based on *a posteriori* information obtained from the image data to be processed. The least squares estimate of α, $\hat{\alpha}_{LS}$ for model (1) is given by

$$\hat{\alpha}_{LS} = (\mathbf{M}^T\mathbf{M})^{-1}\mathbf{M}^T\mathbf{r} \tag{5}$$

and the LS classifier, denoted by P_{LS}, is given by

$$P_{\mathrm{LS}}(\mathbf{r}) = (\mathbf{d}^T P_{\mathbf{U}}^{\perp}\mathbf{d})^{-1} P_{\mathrm{OSP}}(\mathbf{r}). \tag{6}$$

IV. Partially Constrained LSMA Methods

The P_{LS} classifier specified by (6) imposed no constraints on the abundance vector $\alpha = (\alpha_1\ \alpha_2 \cdots \alpha_p)^T$. Therefore, it only provides a suboptimal solution. In order to find a constrained version of P_{LS}, we first consider a partially constrained least squares linear mixing problem that imposes only the ASC on α, then derive the sum-to-one constrained least squares (SCLS) method.

A. SCLS Method

Imposing the ASC on (1) results in the following SCLS linear mixing problem:

$$\min_{\alpha\in\Delta}\{(\mathbf{r}-\mathbf{M}\alpha)^T(\mathbf{r}-\mathbf{M}\alpha)\} \text{ subject to } \Delta = \left\{\alpha \left| \sum_{j=1}^{p} \alpha_j = 1 \right.\right\}. \tag{7}$$

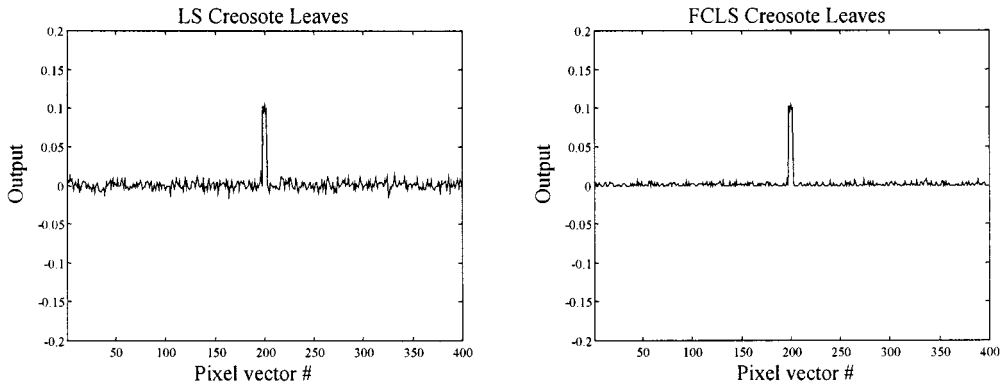

Fig. 2. Results of the LS and FCLS methods in detection and quantification of creosote leaves, where $\mathbf{M}$ consisted of three materials: dry grass, red soil, and creosote leaves.

The solution $\hat{\alpha}_{SCLS}$ to (7) can be obtained by

$$\hat{\alpha}_{SCLS} = P^{\perp}_{\mathbf{M},\mathbf{1}}\hat{\alpha}_{LS} + (\mathbf{M}^T\mathbf{M})^{-1}\mathbf{1}[\mathbf{1}^T(\mathbf{M}^T\mathbf{M})^{-1}\mathbf{1}]^{-1} \quad (8)$$

where $\hat{\alpha}_{LS}$ is given by (5) and

$$P^{\perp}_{\mathbf{M},\mathbf{1}} = \mathbf{I} - (\mathbf{M}^T\mathbf{M})^{-1}\mathbf{1}[\mathbf{1}^T(\mathbf{M}^T\mathbf{M})^{-1}\mathbf{1}]^{-1}\mathbf{1}^T \quad (9)$$

with $\mathbf{1} = (\underbrace{1, 1, \cdots, 1}_{p})^T$. Note that the same solution given by (8) was also derived in [27].

Since the SCLS method is based only on the constraint $\Sigma_{j=1}^{p}\ \alpha_j = 1$, its solution $\hat{\alpha}_{SCLS}$ does not guarantee the estimated abundance fractions are nonnegative, i.e., $\alpha_j \geq 0$ for each $1 \leq j \leq p$. In the following section, we consider imposing the ANC ($\alpha_j \geq 0$ for each $1 \leq j \leq p$) on linear mixing problems while discarding the ASC.

B. Nonnegativity Constrained Least Squares (NCLS) Method

Unlike the SCLS method which produces a closed-form solution, the NCLS method does not have an analytical solution since the ANC is formed by a set of p linear inequalities rather than equalities. In general, an NCLS problem can be described by the following optimization problem:

$$\begin{aligned} &\text{Minimize LSE} = (\mathbf{M}\alpha - \mathbf{r})^T(\mathbf{M}\alpha - \mathbf{r}) \text{ over } \alpha \\ &\qquad\qquad \text{subject to } \alpha \geq 0 \end{aligned} \quad (10)$$

where the LSE is used as the criterion for optimality and $\alpha \geq 0$ represents the nonnegativity constraint $\alpha_j \geq 0$ for all $1 \leq j \leq p$. Since $\alpha \geq 0$ is a set of inequalities, the Lagrange multiplier method is not applicable to solving optimal solutions. In order to mitigate this dilemma, we introduce an unknown p-dimensional positive constraint constant vector $\mathbf{c} = (c_1, c_2, \cdots, c_p)^T$ with $c_j > 0$ for $1 \leq j \leq p$ to take care of the nonnegativity constraint. Through $\mathbf{c}$, we can form a Lagrangian J as follows:

$$J = \tfrac{1}{2}(\mathbf{M}\alpha - \mathbf{r})^T(\mathbf{M}\alpha - \mathbf{r}) + \lambda(\alpha - \mathbf{c}) \quad (11)$$

with $\alpha = \mathbf{c}$ and

$$\left.\frac{\partial J}{\partial \alpha}\right|_{\hat{\alpha}_{NCLS}} = 0 \Rightarrow \mathbf{M}^T\mathbf{M}\hat{\alpha}_{NCLS} - \mathbf{M}^T\mathbf{r} + \lambda = 0 \quad (12)$$

which results in the following two iterative equations given by

$$\begin{aligned} \hat{\alpha}_{NCLS} &= (\mathbf{M}^T\mathbf{M})^{-1}\mathbf{M}^T\mathbf{r} - (\mathbf{M}^T\mathbf{M})^{-1}\lambda \\ &= \hat{\alpha}_{LS} - (\mathbf{M}^T\mathbf{M})^{-1}\lambda \end{aligned} \quad (13)$$

and

$$\lambda = \mathbf{M}^T(\mathbf{r} - \mathbf{M}\hat{\alpha}_{NCLS}). \quad (14)$$

These can be used to solve the optimal solution $\hat{\alpha}_{NCLS}$ and the Lagrange multiplier vector $\lambda = (\lambda_1, \lambda_2, \cdots \lambda_p)^T$.

In order to solve the NCLS problem, an iterative algorithm proposed in [30] can be used to generate the solution to (10). Two index sets, called a passive set P consisting of all indices corresponding to positive components in the estimate $\hat{\alpha}_{LS}$ given by (5) and an active set R containing all indices corresponding to negative (or zero) components in the estimate $\hat{\alpha}_{LS}$ were used to iterate (13) and (14). It was shown in [32] that when an optimal NCLS solution was found, the Lagrange multiplier vector λ must satisfy the following Kuhn-Tucker conditions:

$$\begin{aligned} \lambda_j &= 0, \qquad j \in P \\ \lambda_j &< 0 \qquad j \in R. \end{aligned} \quad (15)$$

Using the conditions given by (15), the NCLS algorithm in [30] can effectively select a passive set P from the p material signatures for unmixing. It is this selection process that makes the ANC so important and advantageous to the performance of NCLS and FCLS methods. Simulations and real data experiments conducted in Section VII will demonstrate the significance of the ANC. We refer the details of the NCLS algorithm implementation to [30].

It is worth noting that a more general form of a weighted least squares problem can be considered by replacing the LSE in (11) with

$$(\mathbf{M}\alpha - \mathbf{r})^T\mathbf{W}(\mathbf{M}\alpha - \mathbf{r}) \quad (16)$$

where $\mathbf{W}$ is introduced as a loading factor matrix to weight the significance of each band. For example, $\mathbf{W}$ can be chosen to be the inverse of the noise covariance matrix or a diagonal matrix.

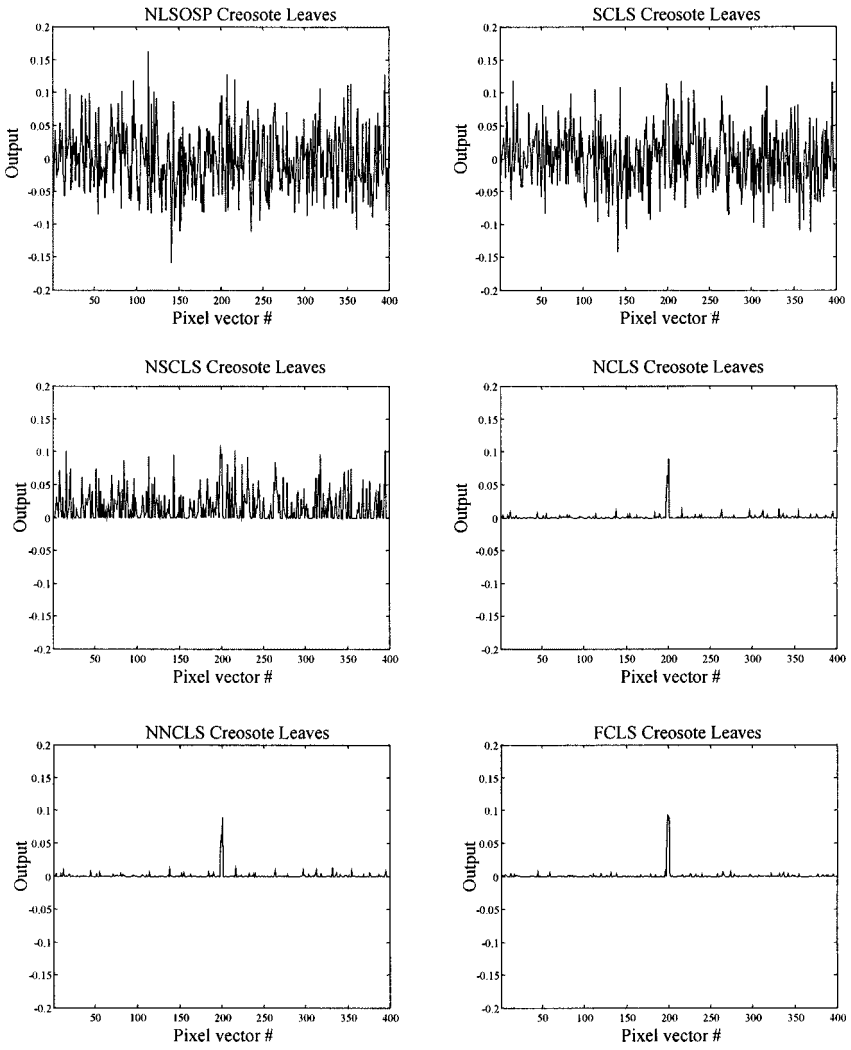

Fig. 3. Results of LS, SCLS, NSCLS, NCLS, NNCLS, and FCLS methods in detection and quantification of creosote leaves, where M consisted of five materials: dry grass, red soil, creosote leaves, sagebrush, and blackbrush.

V. FCLS Method and Unsupervised FCLS Methods

One simple approach to solving for fully constrained linear mixing problems is to take advantage of partially constrained solutions. For an SCLS solution, we simply throw out the material signatures with negative abundance fractions and normalize the abundance fractions of the remaining material signatures to unity. The resulting solution is called a normalized SCLS (NSCLS) solution. For an NCLS solution, we can normalize it to unity, which results in the normalized NCLS (NNCLS) solution. Unfortunately, as will be shown in the experiments, neither the NSCLS nor the NNCLS method will yield optimal solutions since the ANC and the ASC are carried out in sequence and not simultaneously. A method that simultaneously implemented ANC and ASC was recently proposed in [31]. However, it still produced only a nearly optimal solution because it did not satisfy (15). In this section, we present an FCLS algorithm that will generate an optimal solution by making use of the NCLS algorithm developed in the previous section in conjunction with the ASC. Simultaneously requiring both the ASC and the ANC allows us to use the proposed FCLS algorithm to find accurate material signature abundance fractions in a linear mixture. The FCLS method is the same one considered in [32] that extended the nonnegative least squares algorithm in [33] by including the ASC.

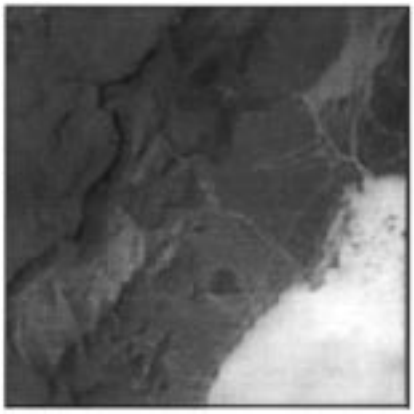

Fig. 4. The 200 × 200 pixel subsection of an AVIRIS image scene (Lunar Crater Volcanic Field).

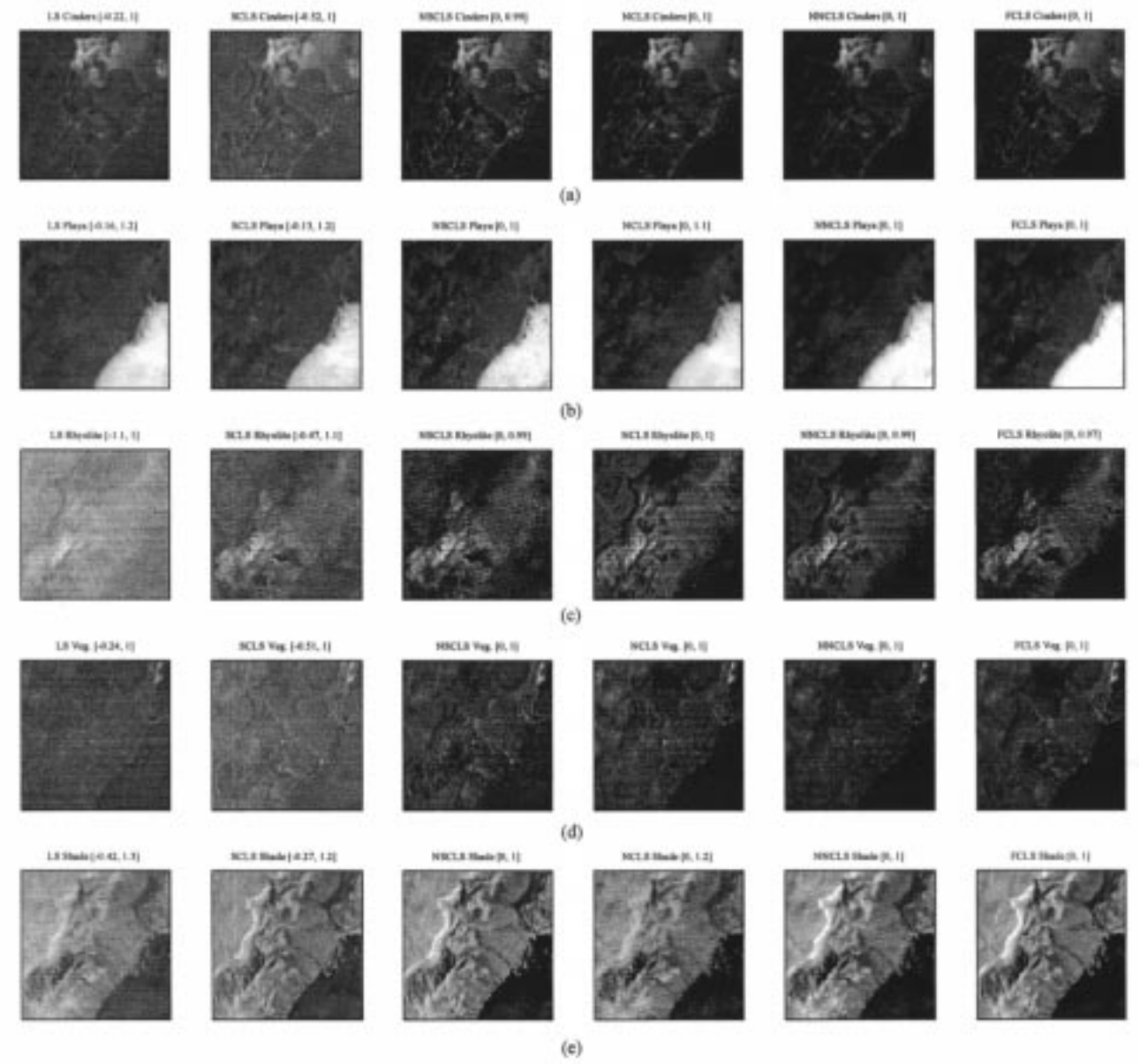

Fig. 5. Results of LS, SCLC, NSCLS, NCLS, NNCLS, and FCLS methods, where figures labeled by (a), (b), (c), (d), and (e) are detection and quantification results of cinders, playa, rhyolite, vegetation, and shade, respectively.

A. FCLS Method

In order to take care of the ASC, we include the ASC in the signature matrix $\mathbf{M}$ by introducing a new signature matrix, denoted by $\mathbf{N}$, defined by

$$\mathbf{N} = \begin{bmatrix} \delta\mathbf{M} \\ \mathbf{1}^T \end{bmatrix} \tag{17}$$

with $\mathbf{1} = \underbrace{(1, 1, \cdots, 1)}_{p}^{T}$ and a vector $\mathbf{s}$ by

$$\mathbf{s} = \begin{bmatrix} \delta\mathbf{r} \\ 1 \end{bmatrix}. \tag{18}$$

The utilization of δ in (17), (18) controls the impact of the ASC. Using these two equations, an FCLS algorithm can be derived directly from the NCLS algorithm described in the previous section by replacing $\mathbf{M}$ and $\mathbf{r}$ used in the NCLS algorithm with $\mathbf{N}$ and $\mathbf{s}$.

B. Unsupervised FCLS Method

The FCLS method requires a complete knowledge of the material signature matrix $\mathbf{M}$. In order for it to apply to a situation where no *a priori* information is available, we need an unsupervised process to generate the required material information to apply the FCLS method. Two criteria were previously developed for this purpose. One was the nearest neighbor rule, from which an unsupervised vector quantization method was derived to find unknown material or signals in an image scene [24]. Another is the target generation process proposed in [34], [35], which was based on the principle of orthogonality. In this section, we propose an LSE-based criterion as an alternative because the methods studied in this paper are also based on the least squares approach. The LSE criterion minimizes the goodness of fit between the linear mixture model and estimated measurements. The idea can be described as follows.

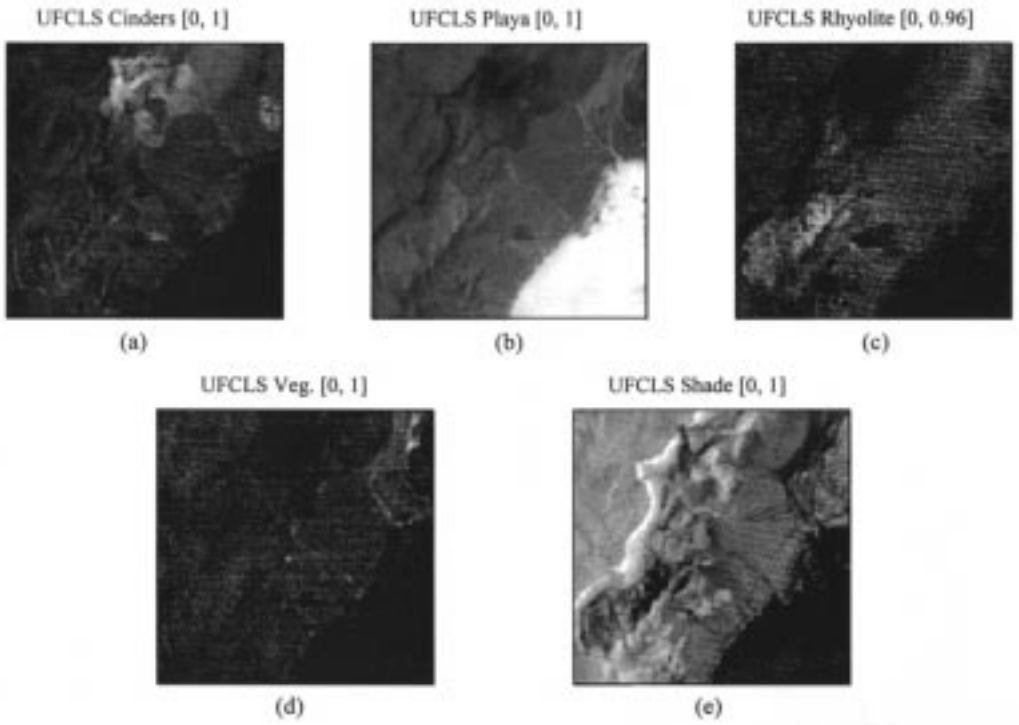

Fig. 6. Results of UFCLS method for (a) cinders, (b) playa, (c) rhyolite, (d) vegetation, and (e) shade with partial material knowledge, where for each image only the material of interest was known *a priori*.

Initially, we make an attempt to select a pure pixel vector of a material present in the image scene as an initial desired material signature denoted by $\mathbf{m}_0$. If there is knowledge of a material signature available *a priori*, then it can become $\mathbf{m}_0$. Also, the initial material signature $\mathbf{m}_0$ is not necessarily limited to one signature. If there is a set of material signatures known to be in the image scene, then these signatures can be formed as an initial material signature set. However, when there is no prior information available about materials, a good choice may be the pixel vector with the maximum length, which is the brightest pixel in the image scene. One reason for this selection is based on the simple fact that the brightest pixel may correspond to a pixel containing a material with the largest radiance spectrum in the image scene. Another reason is because the LSE measures the Euclidean distance, i.e., length between the linear mixture model and a target material pixel. In this case, the initial material pixel and the pixel that has the maximum distance from it tend to be a pair of the brightest and darkest pixels. So, if the brightest pixel is not selected as an initial material pixel, it most likely will be picked in a subsequent selection. Nevertheless, this does not have to be the only way to make the initial selection. Once the initial material pixel is selected, we then assume that all pixel vectors in an image scene are pure pixels made up of $\mathbf{m}_0$ with 100% abundance. Of course, this is generally not true, so we find a pixel vector that has the largest LSE between itself and $\mathbf{m}_0$ and select it as the second material pixel denoted by $\mathbf{m}_1$. Because the LSE between $\mathbf{m}_0$ and $\mathbf{m}_1$ is the largest, it can be expected that $\mathbf{m}_1$ is most distinct from $\mathbf{m}_0$. We then form a material signature matrix $\mathbf{M} = [\mathbf{m}_0\ \mathbf{m}_1]$ and create the matrix $\mathbf{N}$ and $\mathbf{s}$ using (17) and (18). The FCLS algorithm is used to estimate the abundance fractions for $\mathbf{m}_0$ and $\mathbf{m}_1$, denoted by $\hat{\alpha}_0^{(1)}(\mathbf{r})$ and $\hat{\alpha}_1^{(1)}(\mathbf{r})$ for each pixel vector $\mathbf{r}$, respectively. Here, $\mathbf{r}$ is included in the estimated abundance fractions $\hat{\alpha}_0^{(1)}(\mathbf{r})$ and $\hat{\alpha}_1^{(1)}(\mathbf{r})$ to emphasize that $\hat{\alpha}_0^{(1)}(\mathbf{r})$ and $\hat{\alpha}_1^{(1)}(\mathbf{r})$ are functions of $\mathbf{r}$, and they vary with $\mathbf{r}$. The superscript indicates the number of iterations currently being executed. Using $\hat{\alpha}_0^{(1)}(\mathbf{r})$ and $\hat{\alpha}_1^{(1)}(\mathbf{r})$, we then calculate the least squares error (LSE) between $\mathbf{r}$ and its estimated linear mixture $\hat{\alpha}_0^{(1)}(\mathbf{r})\mathbf{m}_0 + \hat{\alpha}_1^{(1)}(\mathbf{r})\mathbf{m}_1$ for all image pixel vectors $\mathbf{r}$. A pixel that yields the largest LSE will be selected to be the third material pixel $\mathbf{m}_2$. The same procedure of using the FCLS algorithm with $\mathbf{M} = [\mathbf{m}_0\ \mathbf{m}_1\ \mathbf{m}_2]$ is repeated until the resulting LSE is small enough and below a prescribed error threshold. Techniques for determining the error threshold will be discussed in Section VII. The procedure outlined as above is called Unsupervised FCLS (UFCLS) Algorithm, which can be summarized as follows.

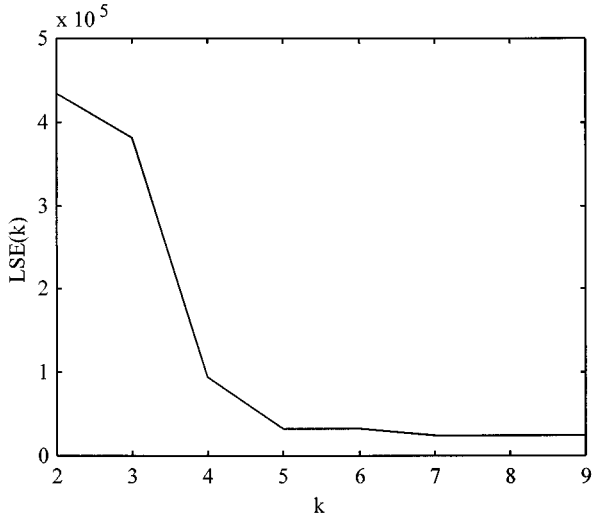

Fig. 7. Plot of maximum LSE values: $\mathrm{LSE}^{(k)}(\mathbf{r})$ for AVIRIS image.

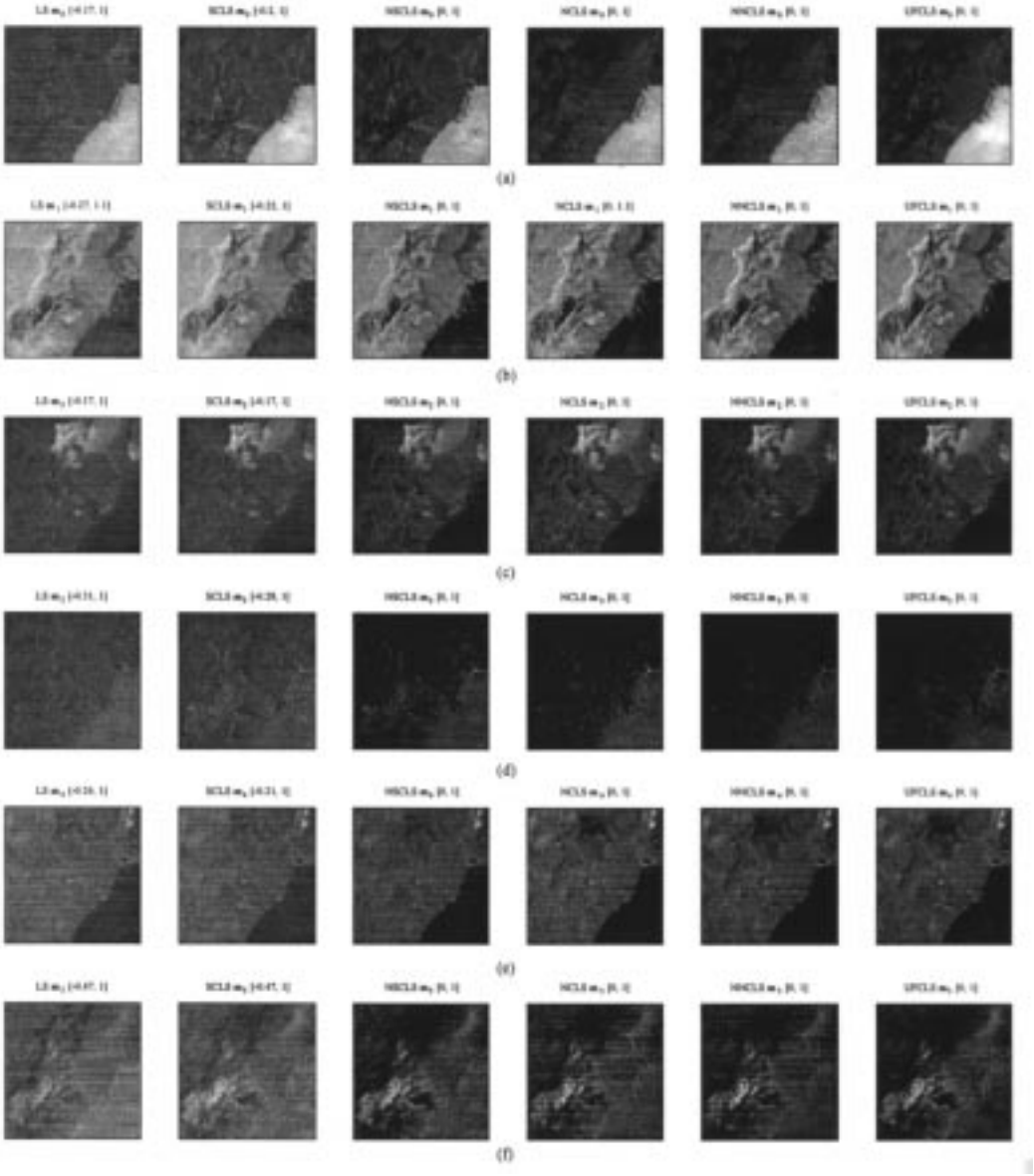

Fig. 8. Resulting $\mathrm{LSE}^{(k)}(\mathbf{r})$ images (a) $k = 0$, (b) $k = 1$, (c) $k = 2$, (d) $k = 3$, (e) $k = 4$, and (f) $k = 5$.

Unsupervised FCLS (UFCLS) Algorithm:

1) Initial condition:
Select ε to be a prescribed error threshold, and let $\mathbf{m}_0 = \arg\{\max_{\mathbf{r}} [\mathbf{r}^T\mathbf{r}]\}$ where $\mathbf{r}$ is run over all image pixel vectors. Let $k = 0$.

2) Find $\mathbf{m}_1$ that yields the largest $\mathrm{LSE}^{(0)}(\mathbf{r}) = (\mathbf{r}-\mathbf{m}_0)^T(\mathbf{r}-\mathbf{m}_0)$, i.e., $\mathbf{m}_1 = \arg\{\max_{\mathbf{r}} \mathrm{LSE}^{(0)}(\mathbf{r})\}$.

3) Let $k \leftarrow k+1$, and apply the FCLS algorithm with the signature matrix $\mathbf{M} = [\mathbf{m}_0\ \mathbf{m}_1 \cdots \mathbf{m}_k]$, $\mathbf{N} = \begin{bmatrix}\delta\mathbf{M} \\ \mathbf{1}^T\end{bmatrix}$ and $\mathbf{s} = \begin{bmatrix}\delta\mathbf{r} \\ 1\end{bmatrix}$ to estimate the abundance fractions of $\mathbf{m}_0$, $\mathbf{m}_1$, $\cdots, \mathbf{m}_k$, $\hat{\alpha}_0^{(k)}(\mathbf{r})$, $\hat{\alpha}_1^{(k)}(\mathbf{r})$, and $\cdots, \hat{\alpha}_{k-1}^{(k)}(\mathbf{r})$.

4) Find the least squares error defined by

$$\mathrm{LSE}^{(k)}(\mathbf{r}) = \left(\mathbf{r} - \left[\sum_{i=0}^{k} \hat{\alpha}_i^{(k)}(\mathbf{r})\mathbf{m}_i\right]\right)^T \cdot \left(\mathbf{r} - \left[\sum_{i=0}^{k} \hat{\alpha}_i^{(k)}(\mathbf{r})\mathbf{m}_i\right]\right) \tag{19}$$

and check the error if $\mathrm{LSE}^{(k)}(\mathbf{r}) < \varepsilon$ for all $\mathbf{r}$. If it is, the algorithm stops, otherwise continue.

5) Find $\mathbf{m}_{k+1} = \arg\{\max_{\mathbf{r}} \mathrm{LSE}^{(k)}(\mathbf{r})\}$. Go to step 3.

It should be noted that $\{\mathrm{LSE}^{(k)}(\mathbf{r})\}$ is a monotonically decreasing sequence at k, thus, it converges. Additionally, an analogous approach to UFCLS can also be used to extend LS, SCLS, NSCLS, NCLS, and NNCLS methods to Unsupervised LS, Unsupervised SCLS, Unsupervised NSCLS, Unsupervised NCLS, and Unsupervised NNCLS [36].

VI. Computer Simulations and Experiments

This section contains a series of computer simulations and experiments to evaluate comparative performance of the LS, SCLS, NSCLS, NCLS, NNCLS, and FCLS methods and their corresponding unsupervised versions. First, we conducted computer simulations to demonstrate advantages of the FCLS and

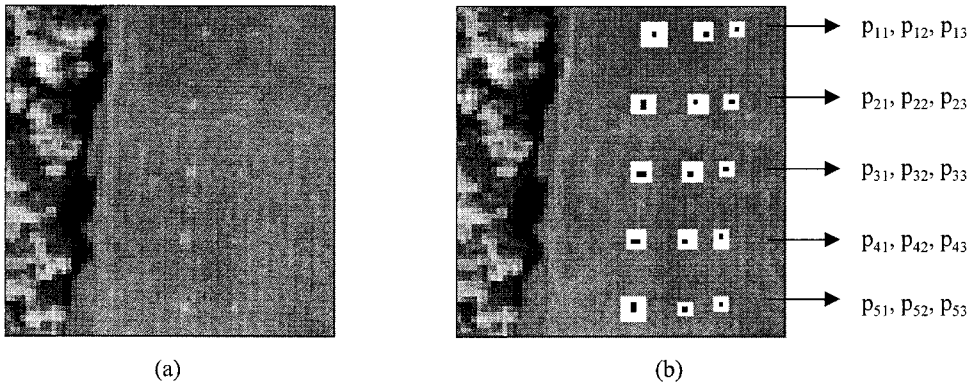

Fig. 9. Results of LS, SCLS, NSCLS, NCLS, NNCLS, and UFCLS methods using material pixels generated by the UFCLS algorithm.

UFCLS methods. Then real hyperspectral image data were used to show the superior performance of the FCLS and UFCLS methods in comparison to other methods. In implementing the FCLS and UFCLS methods, the value of δ used in (17) and (18) was fixed at $\delta = 1.0 \times 10^{-5}$, except for HYDICE experiments where various δ values were explored for study.

A. Computer Simulations

In the following simulations, two experiments were designed to demonstrate the performance of the LS, SCLS, NSCLS, NCLS, NNCLS, and FCLS methods 1) when the information of all material signatures is completely known, and 2) when some false information is used.

Example 1: Signature Matrix with Three Distinct Material Signatures: A set of reflectance spectra considered in [22] was used for performance evaluation. The set contained five reflectance spectra, dry grass, red soil, creosote leaves, blackbrush, and sagebrush. These spectra were convolved to 10 nm spectral bands and atmospheric water bands were removed, as shown in Fig. 1. A signature matrix $\mathbf{M}$ was formed from the dry grass, red soil, and creosote leaves signatures $\mathbf{M} = [\mathbf{m}_1\ \mathbf{m}_2\ \mathbf{m}_3]$, with their associated abundance fractions given by $\alpha = (\alpha_1, \alpha_2, \alpha_3)^T$. The simulation consisted of 400 mixed pixel vectors. We started the first pixel vector with 100% red soil and 0% dry grass, then began to increase 0.25% dry grass and decrease 0.25% red soil every pixel vector until the 400th pixel vector, which contained 100% dry grass. We then added creosote leaves to pixel vector numbers 198–202 at abundance fractions 10%, while reducing the abundance of red soil and dry grass by multiplying their abundance fractions by 90%. For example, after the addition of creosote leaves, the resulting pixel vector 200 contained 10% creosote leaves, 45% red soil, and 45% dry grass. White Gaussian noise was also added to each pixel vector to achieve a 30:1 SNR, which was defined in [22] as 50% reflectance divided by the standard deviation of the noise. It should be noted that the NCLS method was shown in [30] to be an effective constrained subpixel target detector where this simulation example was used to evaluate its performance in target detection. In this experiment, the same set of simulated pixel vectors was also used to evaluate the quantification performance of the NCLS method compared to other methods. Since all six methods performed similarly, only results in detection of creosote leaves from the worst (LS) and the best (FCLS) are shown in Fig. 2. In order to further compare their capabilities at quantifying creosote leaves, the squared errors between the actual and estimated abundance fractions of creosote leaves were averaged over 400 pixels. The resulting quantification errors for

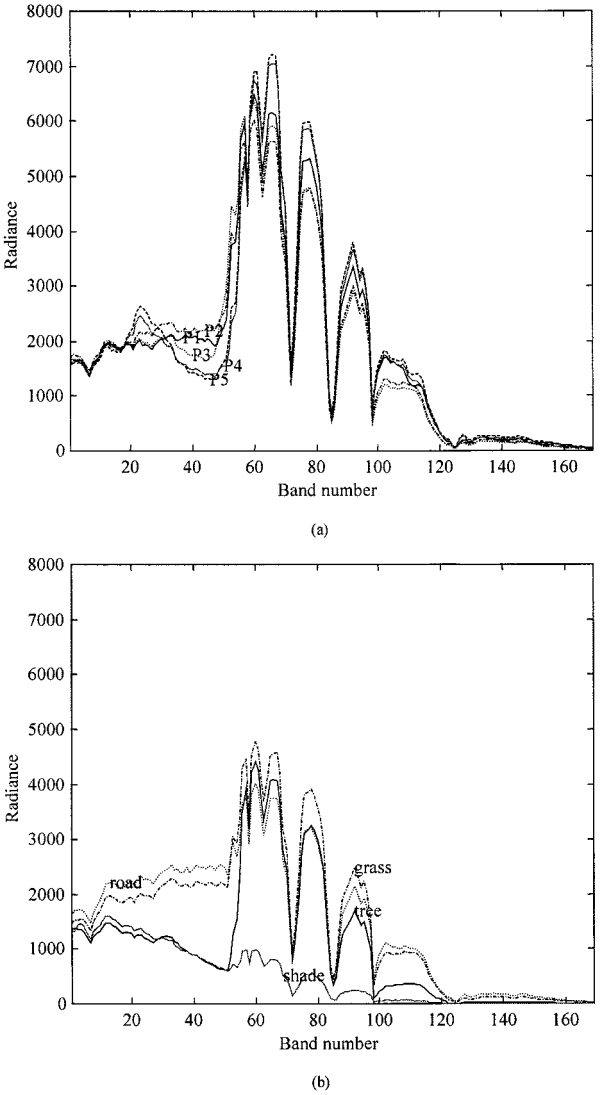

Fig. 10. HYDICE Forest Radiance data. (a) The 64 × 64 pixel subsection of a HYDICE image scene and (b) target locations.

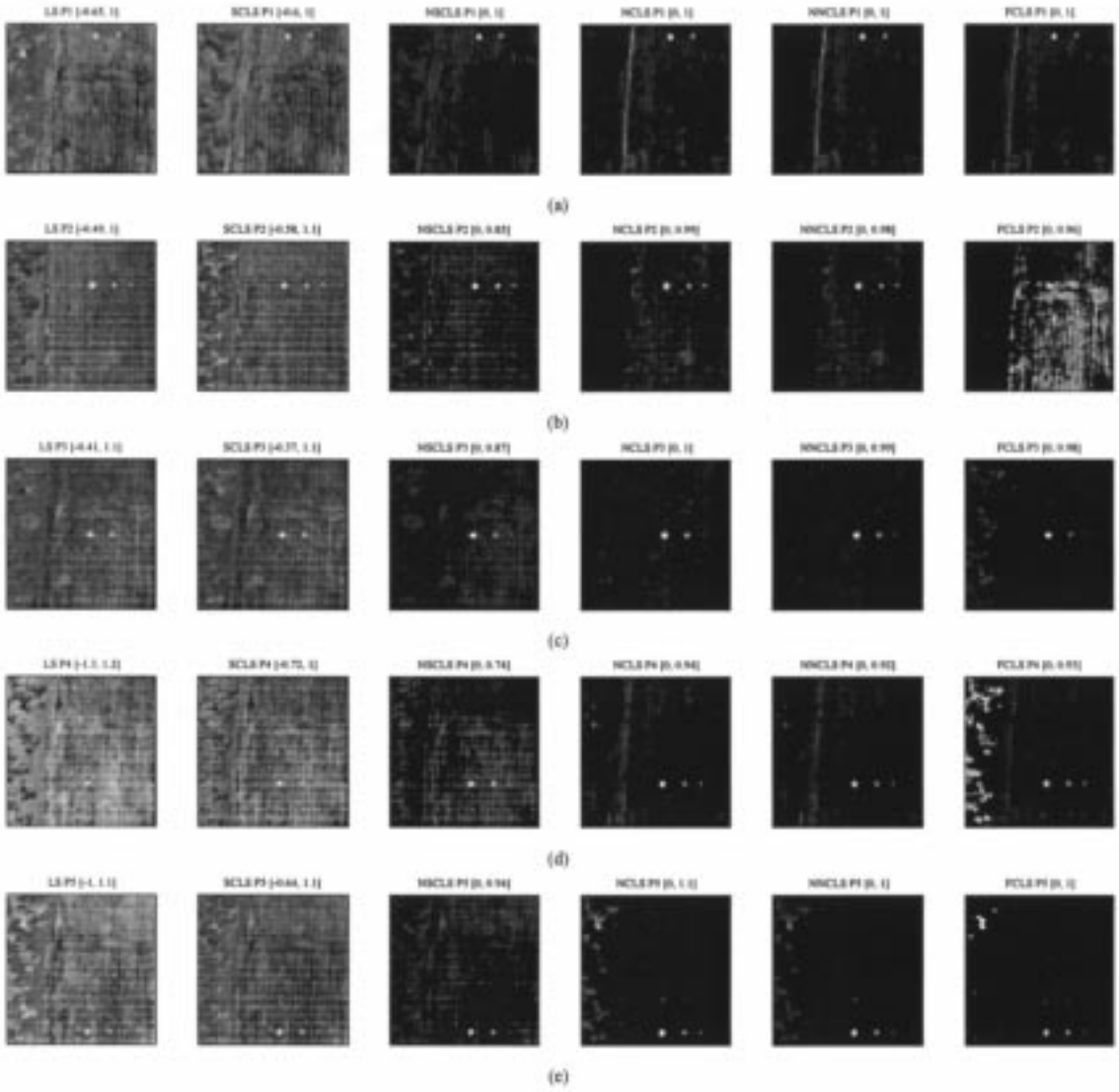

Fig. 11. Results of LS, SCLS, NSCLS, NCLS, NNCLS, and FCLS methods, where figures labeled by (a), (b), (c), (d), and (e) are detection and quantification results of P1, P2, P3, P4, and P5, respectively.

each method were 2.588 $\times$ 10^{-5} for LS, 7.850 $\times 10^{-6}$ for SCLS, 3.717 $\times$ 10^{-6} for NSCLS, 1.318 $\times 10^{-5}$ for NCLS, 1.303 $\times 10^{-5}$ for NNCLS, and 3.715 $\times 10^{-6}$ for FCLS. Obviously, the FCLS method produced the best quantification result in the sense of minimizing the average of squared errors. It is interesting to note that NSCLS and FCLS methods performed nearly the same. However, this will not be true in following simulation.

Example 2: Effects of Two Additional, Less Spectrally Distinct, Materials: The material signature matrix $\mathbf{M}$ is made up of the spectral signatures of all materials in the image scene. An image pixel may not necessarily contain all these materials and may contain only one or a mixture of only a few of them. In order to demonstrate the effects of some materials used in $\mathbf{M}$, but absent in a pixel, the same simulated mixed pixel vectors used in Section A-1 were used. However, two additional signatures, blackbrush and sagebrush, were added to the signature matrix $\mathbf{M}$. These signatures were not actually present in the pixel vectors, that is, the abundance fractions of blackbrush and sagebrush in these 400 simulated pixels was 0%. In this scenario, the signature matrix $\mathbf{M} = [\mathbf{m}_1\ \mathbf{m}_2\ \mathbf{m}_3\ \mathbf{m}_4\ \mathbf{m}_5]$ was assumed to consist of these five spectral signatures with abundance fractions given by $\alpha = (\alpha_1, \alpha_2, \alpha_3, \alpha_4, \alpha_5)^T$. Fig. 3 shows the results of the LS, SCLS, NSCLS, NCLS, NNCLS, and FCLS methods in detection of creosote leaves. Unlike Fig. 2, the performance of the LS, SCLS, and NSCLS methods was very poor and their respective averaged squared quantification errors 2.556 $\times$ 10^{-3} for the LS, 1.945 $\times$ 10^{-3} for the SCLS, 7.960 $\times$ 10^{-4} for the NSCLS were significantly worse than those produced by the other three methods, 4.823 $\times$ 10^{-5} for the NCLS, 4.907 $\times$ 10^{-5} for the NNCLS, and 2.806 $\times$ 10^{-5} for the FCLS. The detection performance of the LS method was considerably decreased because the undesired signature annihilator $P_{\mathbf{U}}^{\perp}$ used in this method nulled the undesired signatures, blackbrush and sagebrush whose spectra are similar to that of creosote leaves. The performance of the SCLS and NSCLS methods was reduced because they assumed there were five signatures and their estimated abundance fractions must be

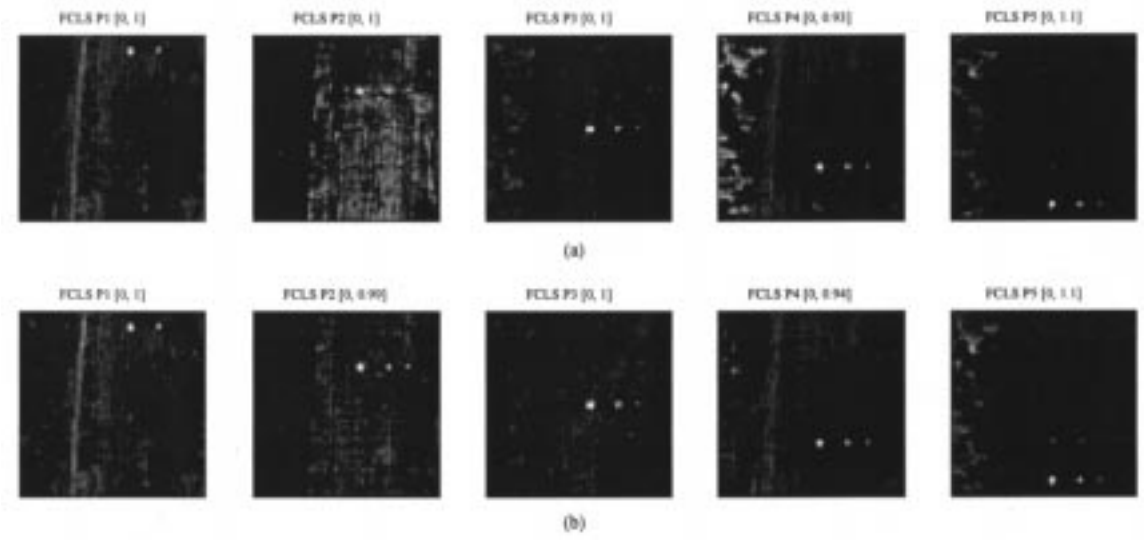

Fig. 12. Results of FCLS methods. (a) $\delta = 1.0 \times 10^{-4}$ and (b) $\delta = 1.0 \times 10^{-2}$.

TABLE I
SUM OF QUANTIFICATION RESULTS OVER ALL IMAGE PIXELS FOR LS, SCLS, NSCLS, NCLS, NNSCLS, AND FCLS METHODS USING MANUALLY SELECTED BACKGROUND SIGNATURES

	LS	SCLS	NSCLS	NCLS	NNCLS	FCLS δ = 1 x 10^{-5}	FCLS δ = 1 x 10^{-4}	FCLS δ = 1 x 10^{-2}
P1	-73.97	-67.72	143.35	106.30	105.94	107.97	109.18	106.30
P2	60.05	53.66	152.40	67.29	64.31	608.29	355.33	67.33
P3	28.37	27.08	112.67	24.02	22.90	36.66	28.41	24.02
P4	137.45	129.06	215.44	44.34	45.48	169.11	123.00	44.34
P5	-101.32	-94.71	139.41	53.93	41.89	26.38	36.59	53.94

TABLE II
SUM OF QUANTIFICATION RESULTS OVER ONLY BLACK AND WHITE-MASKED PIXELS FOR LS, SCLS, NSCLS, NCLS, NNSCLS, AND FCLS METHODS USING MANUALLY SELECTED BACKGROUND SIGNATURES

	LS	SCLS	NSCLS	NCLS	NNCLS	FCLS δ = 1 x 10^{-5}	FCLS δ = 1 x 10^{-4}	FCLS δ = 1 x 10^{-2}
P_{11}	5.99	4.26	3.70	4.08	4.08	4.11	4.11	4.08
P_{12}	3.01	2.09	1.83	1.70	1.69	1.71	1.70	1.70
P_{13}	0.50	-1.01	0.01	0.05	0.05	0.00	0.01	0.05
P_{21}	5.89	4.75	4.03	4.74	4.66	7.67	6.40	4.74
P_{22}	0.30	1.40	1.68	1.36	1.30	7.48	4.71	1.36
P_{23}	-0.02	0.96	0.78	0.73	0.71	2.49	1.75	0.73
P_{31}	4.39	4.61	3.62	4.59	4.53	3.87	4.14	4.59
P_{32}	3.86	3.80	2.40	1.76	1.71	1.01	1.25	1.76
P_{33}	1.28	1.44	0.95	0.58	0.56	0.34	0.39	0.58
P_{41}	4.53	5.89	4.03	3.16	3.05	3.49	3.62	3.16
P_{42}	8.66	5.91	3.78	1.46	1.44	1.50	1.62	1.46
P_{43}	3.48	3.59	2.05	0.44	0.43	0.46	0.43	0.44
P_{51}	-0.10	-0.07	3.10	4.12	3.94	3.67	3.61	4.12
P_{52}	0.25	0.75	1.08	1.82	1.81	1.70	1.82	1.82
P_{53}	-1.21	-0.88	0.13	0.41	0.40	0.26	0.35	0.41

summed to one. Since the spectrum of creosote leaves is close to those of blackbrush and sagebrush, the estimated abundance fraction of creosote leaves was forced to share with the nonexistent blackbrush and sagebrush. As expected, the SCLS and NSCLS methods would not perform well. In contrast, the ANC significantly improved the performance of the NCLS, NNCLS, and FCLS methods. By implementing the ANC, these methods were able to effectively select an appropriate subset of material signatures for unmixing. This experiment demonstrated that the NCLS, NNCLS, and FCLS methods performed significantly better than the LS, SCLS, and NSCLS methods as the number and similarity of spectral signatures in the signature matrix M increases. In both examples, the FCLS method performed the best while the LS method was the worst.

B. AVIRIS and HYDICE Hyperspectral Image Experiments

Example 3: AVIRIS data: The data used in the following experiments are from the AVIRIS sensor and were the same data considered in [22]. It is an AVIRIS scene of 200 × 200 pixels of the Lunar Crater Volcanic Field in Northern Nye County, Nevada shown in Fig. 4. There are five signatures of interest in this image: red oxidized basaltic "cinders," "rhyolite," "playa (dry lakebed)," "vegetation," and "shade." For this experiment, representative pixels of each signature were manually extracted from the image scene and their average was used to represent the signature. The signature for the playa was obtained by averaging 5033 pixels located at the bottom right corner of the image scene. The shade signature was generated by averaging pixels in a 5 × 5 square located in the darkest area of the scene. Each of the signatures for cinders and rhyolite was produced by averaging four pixels in the scene and one pixel was extracted for a vegetation signature. Three experiments were conducted using different degrees of prior signature information.

Experiment 1: Complete Prior Signature Information: Using these five manually selected signatures, a signature matrix $\mathbf{M}$ was formed. Fig. 5 shows the quantification results of LS, SCLS, NSCLS, NCLS, NNCLS, and FCLS methods where figures labeled (a)–(e) were generated by using cinders, playa, rhyolite, vegetation, and shade as the desired signatures, respectively. The estimated abundance fraction values for each signature correspond directly to the gray scale values for each image and the range of abundance fraction values for each image is indicated in the image title. As we can see, from a detection point of view, all six methods performed similarly. However, in terms of quantification, the performances of the NSCLS, NCLS, NNCLS, and FCLS methods are very close and better than the LS and SCLS methods.

Experiment 2: Partial Prior Signature Information: In this experiment, only one of five signatures was assumed to be known *a priori*. In this case, the UFCLS algorithm was used to generate additional signatures to form a desired signature matrix M to quantify this particular signature. Fig. 6(a) shows the results of cinders after 16 iterations of the UFCLS algorithm. Similarly, Fig. 6(b)–(e) shows the results of playa, rhyolite, vegetation, and shade after 3, 19, 25, and 5 iterations, respectively. Compared to Fig. 5, both results were very similar.

Experiment 3: No Prior Signature Information: The following experiment is interesting and designed to explore the utility of UFCLS algorithm when no prior information is assumed. In order to initialize the algorithm, a prescribed error threshold ε and an initial material signature $\mathbf{m}_0$ were required. To determine a value for ε, we used the UFCLS algorithm and plotted the maximum LSE values resulting from (19), as shown in Fig. 7. Since the plot leveled off at iteration $k = 5$, a threshold value of 5×10^4 was selected for ε. The UFCLS was performed and resulted in six signatures, $\mathbf{m}_0$, $\mathbf{m}_1$, $\mathbf{m}_2$, $\mathbf{m}_4$, and $\mathbf{m}_5$, which specified playa, shade, cinders, vegetation, and rhyolite, respectively, and $\mathbf{m}_3$, which corresponded to an anomaly that could not identified by visual inspection. This experiment shows that the UFCLS can be used to detect anomalies, a task that cannot be accomplished by the supervised FCLS. These six signatures were then used to form a signature matrix $\mathbf{M}$ for implementation of the LS, SCLS, NSCLS, NCLS, NNCLS, and FCLS methods. The results are shown in Fig. 8. Compared to the images in Fig. 5, the images in Fig. 8 are similar, but quantification results are worse, particularly for playa and shade. This is primarily due to the fact that only a single pixel was used to generate each of signatures in $\mathbf{M}$. When relatively large areas such as dry lakebed and shade need to be classified, a single pixel can not well represent these areas due to their spectral variability. One way to resolve this dilemma is to add more sample pixels to generate a more robust signature. These additional sample pixels can be selected by using spectral measures such as, Euclidean distance [14], spectral angle mapper (SAM) [1] or spectral information divergence (SID) [37], [38].

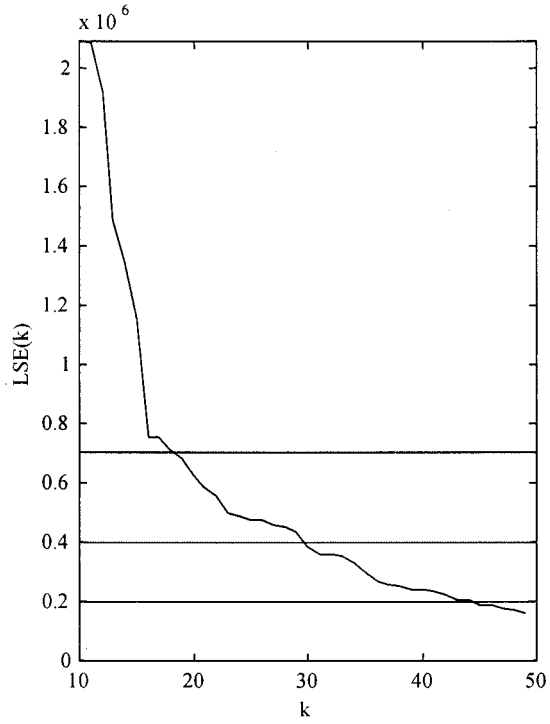

Fig. 13. Plot of maximum LSE values, $\mathrm{LSE}^{(k)}(\mathbf{r})$ for HYDICE image, where prior knowledge of P1, P2, P3, P4, and P5 was assumed.

Example 4: HYDICE data: The data to be used in this example were HYDICE data after geometric correction. The low signal/high noise bands were bands 1–3 and bands 202–210, water vapor absorption bands were bands 101–112, and bands 137–153 were removed. Fig. 9(a) shows a HYDICE image scene of size 64 × 64 with 1.5 m spatial resolution and 10 nm spectral resolution. Fig. 9(b) provides ground truth locations for 15 panels of interest in the scene where the black-masked pixels indicate the panel center pixels, and white-masked pixels indicate pixels that may contain some abundance fraction of a panel. These 15 panels were located in a large grass field and were arranged in a 5 × 3 matrix with each element denoted by p_{ij}, where i is the row index and j is the corresponding column index. For each row $i = 1, \cdots, 5$, and the three panels p_{i1}, p_{i2}, p_{i3} were made of the same material, but have different sizes. For each column j, the five panels $p_{1j}, p_{2j}, p_{3j}, p_{4j}, p_{5j}$ had the same size, but consisted of different materials. The sizes of the panels in the first, second, and third columns are

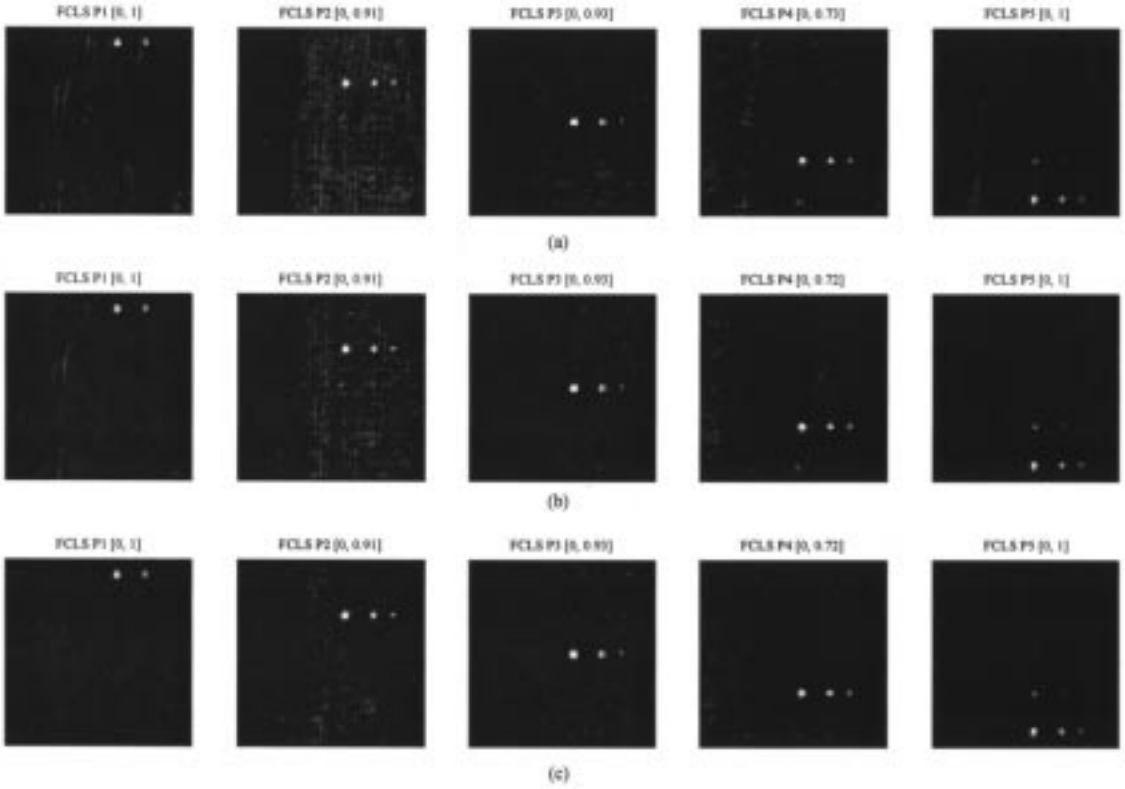

Fig. 14. Results of UFCLS methods, where prior knowledge of P1, P2, P3, P4, and P5 was assumed: (a) $\varepsilon = 7.0 \times 10^5$, (b) $\varepsilon = 4.0 \times 10^5$, (c) $\varepsilon = 2.0 \times 10^5$.

3 m $\times$ 3 m, 2 m $\times$ 2 m, and 1 m $\times$ 1 m, respectively. So, the 15 panels consisted of five different materials and three different sizes. Since panels $p_{11}, p_{21}, p_{31}, p_{41}, p_{51}$ are of size 3 m $\times$ 3 m, the 1.5 m-spatial resolution of the image scene results in at least one image pixel with an abundance fraction of 1.0 for each of these panels.

Experiment 1: Complete Prior Signature Information: In order to form a desired signature matrix for M, the black pixels in the first column of row i were averaged to create a signature, denoted by Pi to represent the signatures of panels in row i. So, there are five panel signatures, P1, P2, P3, P4, and P5. Fig. 10(a) shows the radiance spectra for each of these signatures, where all the panels have very similar spectra. In addition to the panel signatures, four more signatures were generated to represent the background. A tree signature was obtained by averaging 768 pixels in a large rectangle of pixels from the left side of the image. A grass signature was generated by averaging 1152 pixels from two large rectangles, one located between the trees and the panels, and the second at the right side of the image. Averaging eight pixels from the gravel road and seven pixels of shade located along the tree line produced road and shade signatures, respectively. Since most of the road was shaded, it is very difficult to see in Fig. 10. The spectra of these four background signatures are shown in Fig. 10(b). By including the four background signatures with the five panel signatures, a total of nine signatures were used to form $\mathbf{M}$. Fig. 11 shows the performance of the LS, SCLS, NSCLS, NCLS, NNCLS and FCLS methods where figures labeled by (a)–(e) are detection results for panels from rows 1 to 5, respectively. Until now, we have simply set the value of δ at $\delta = 1.0 \times 10^{-5}$ for use in the FCLS and UFCLS methods. In order to demonstrate its effect on performance of the FCLS method, the same experiment was conducted with $\delta = 1.0 \times 10^{-4}$ and $\delta = 1.0 \times 10^{-2}$. These results are shown in Fig. 12. Comparison of these results with those of the NCLS method in Fig. 11 illustrates the increasingly similar performance as the value of δ was increased. This effect was expected, since δ controls the impact of the ASC constraint and a reduction of this impact should correspond to increased similarity between results of the FCLS and NCLS methods.

An advantage of using panels for experiments is that ground truth provides their exact dimensions and we can use this information to quantify the amount of each panel material present in the scene. Since each image pixel is approximately 1.5 m $\times$ 1.5 m, with an area-per-pixel of 2.25 m^2, we can determine the quantity of panel materials by dividing the area of the 3 m $\times$ 3 m, 2 m $\times$ 2 m, and 1 m $\times$ 1 m panels by the area-per-pixel, which results in quantification values 4.0, 1.78, and 0.44 pixels, respectively. Consequently, the image contains a quantity of approximately 6.22 pixels of each panel material. Table I contains the image quantification results for each of the methods. As we can see, each method performed poorly. In order to determine how each of the methods performed in quantification of each of the three panel sizes, Table II contains quantification results for each of the methods using only the black-masked and white-masked pixels of each panel. For instance, the quantification results for p_{11} in row 1 of Table II were calculated using only the 25 pixels corresponding to p_{11}'s black and white mask. These results show that the NCLS, NNCLS, and FCLS ($\delta = 1.0 \times 10^{-2}$) methods performed better than other methods in terms of both detection and quantification.

However, since the large background field was not well represented by the four manually generated background signatures, all the methods performed poorly. As noted, the HYDICE sensor can extract objects as small as 1 m, and consequently, many unknown materials may also be picked up by the sensor. This is indeed the case in Fig. 11. Unfortunately, the knowledge of these unidentified materials cannot be obtained *a priori*. This is a situation where the UFCLS method finds its most useful applications.

Experiment 2: Partial Prior Signature Information: In this experiment, only the five panel signatures were assumed to be known *a priori*. In this case, the UFCLS algorithm was used to generate additional signatures to represent the background. The five panel signatures from Experiment 1 were selected as the initial material signature set to initialize the UFCLS algorithm. It is interesting to note that at iteration 11 the UFCLS algorithm selected the top black-masked pixel for panel P5 as a new material signature. This indicated that one of the two black-masked pixels was actually a mixed pixel. In order to determine which was the mixed pixel, the UFCLS method, with no prior signature knowledge (Experiment 3 in Example 3) was used. It selected a bottom black-masked pixel. Consequently, only the bottom black-masked pixel was used to represent panel P5 in this experiment. As stated before, the UFCLS method requires a prescribed error threshold to determine how many targets will be included in the signature matrix $\mathbf{M}$. In order to determine this value, we used the UFCLS algorithm and plotted the maximum LSE values resulting from (19). Fig. 13 shows the results for iterations of k from 10 to 49. The plot starts to level off after about 18 iterations of the UFCLS algorithm. In order to see how the threshold value effects the UFCLS method, three threshold values (7.0×10^5, 4.0×10^5 and 2.0×10^5) were selected, each of which was thresholded by a horizontal line in Fig. 13. Fig. 14 shows the results of the UFCLS method using these three threshold values. As we can see from Fig. 14(a), when the error threshold is too large it results in an insufficient number of material signatures to represent the image background. Tables III and IV contain quantification results for the entire image and for the black and white-masked pixels respectively. As we can see from the quantification values in these two tables, the UFCLS method using partial prior material knowledge performed significantly better than the FCLS method using manually selected material signatures.

Experiment 3: No Prior Signature Information: The previous experiments assumed that a priori knowledge of the material signatures was available. In this final experiment we conclude by assuming that no prior material knowledge is given. As before, we must prescribe an error threshold value to terminate the UFCLS algorithm. Again, we used the UFCLS algorithm and plotted the maximum LSE values resulting from (19), as shown in Fig. 15(a). In order to determine an appropriate threshold the difference between every fifth sample was calculated using the following equation:

$$\Delta \mathrm{LSE}^{(k)} = \frac{\max_{\mathbf{r}}\{\mathrm{LSE}^{(k-5)}(\mathbf{r})\} - \max_{\mathbf{r}}\{\mathrm{LSE}^{(k)}(\mathbf{r})\}}{\max_{\mathbf{r}}\{\mathrm{LSE}^{(k-5)}(\mathbf{r})\}}. \tag{20}$$

TABLE III
SUM OF QUANTIFICATION RESULTS OVER ALL IMAGE PIXELS USING UFCLS METHOD WITH PARTIAL PRIOR SIGNATURE KNOWLEDGE FOR THREE DIFFERENT ERROR THRESHOLD VALUES

	UFCLS $\varepsilon = 7.0\times10^5$	UFCLS $\varepsilon = 4.0\times10^5$	UFCLS $\varepsilon = 2.0\times10^5$
P1	19.7649	13.9114	7.3021
P2	109.4454	41.2200	19.9960
P3	20.3169	14.8010	23.0000
P4	15.2187	11.5537	9.4493
P5	21.5999	11.2960	10.2822

TABLE IV
SUM OF QUANTIFICATION RESULTS OVER ONLY BLACK AND WHITE-MASKED PIXELS USING UFCLS METHOD WITH PARTIAL PRIOR SIGNATURE KNOWLEDGE FOR THREE DIFFERENT ERROR THRESHOLD VALUES

	UFCLS $\varepsilon = 7.0\times10^5$	UFCLS $\varepsilon = 4.0\times10^5$	UFCLS $\varepsilon = 2.0\times10^5$
P_{11}	3.2691	3.1162	3.0897
P_{12}	1.3128	1.2508	1.2433
P_{13}	0.0413	0.0492	0.0526
P_{21}	4.9350	4.2786	4.2540
P_{22}	2.4201	1.8693	1.6412
P_{23}	1.1844	0.7295	0.5539
P_{31}	3.9199	4.0814	4.3011
P_{32}	1.7502	1.7754	2.0301
P_{33}	0.4203	0.4330	0.5630
P_{41}	2.9124	3.1241	2.9777
P_{42}	1.6915	1.5367	1.7529
P_{43}	0.4634	0.5104	0.4758
P_{51}	3.7763	3.8227	3.9045
P_{52}	1.8771	1.8153	1.8415
P_{53}	0.4937	0.5173	0.4756

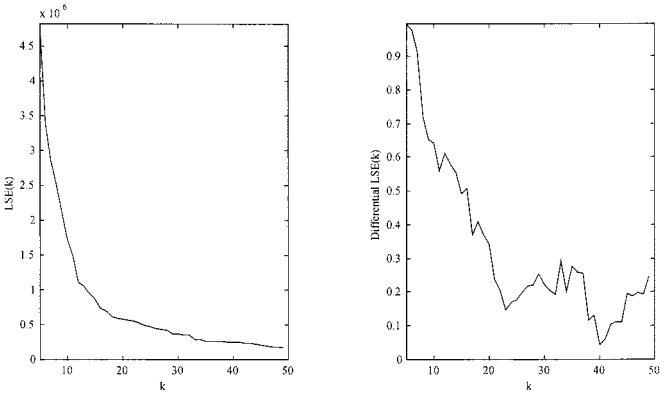

Fig. 15. HYDICE UFCLS error. (a) LSE and (b) differential LSE.

This is the same method used to determine the number of materials or codewords for an unsupervised vector quantization method in [39]. This function is plotted in Fig. 15(b) and shows a significant drop at values of 11, 23, and 40. A prescribed error threshold of $\varepsilon = 2.54 \times 10^5$, which corresponded to the drop at 40 was selected for the UFCLS algorithm and resulted in the generation of 41 signatures. These 41 signatures were used to form a signature matrix $\mathbf{M}$. Using this $\mathbf{M}$, the LS, SCLS, NSCLS, NCLS, and NNCLS methods were implemented. Fig. 16(a)–(f) shows results for $\mathbf{m}_9$, $\mathbf{m}_{33}$, $\mathbf{m}_4$, $\mathbf{m}_{22}$, $\mathbf{m}_{35}$, and $\mathbf{m}_3$ where panel P1, P2, P3, P4, P4, and P5 were detected, respectively. In each case, a black-masked pixel was selected as a material signature, except for $\mathbf{m}_{33}$, which turned out to be

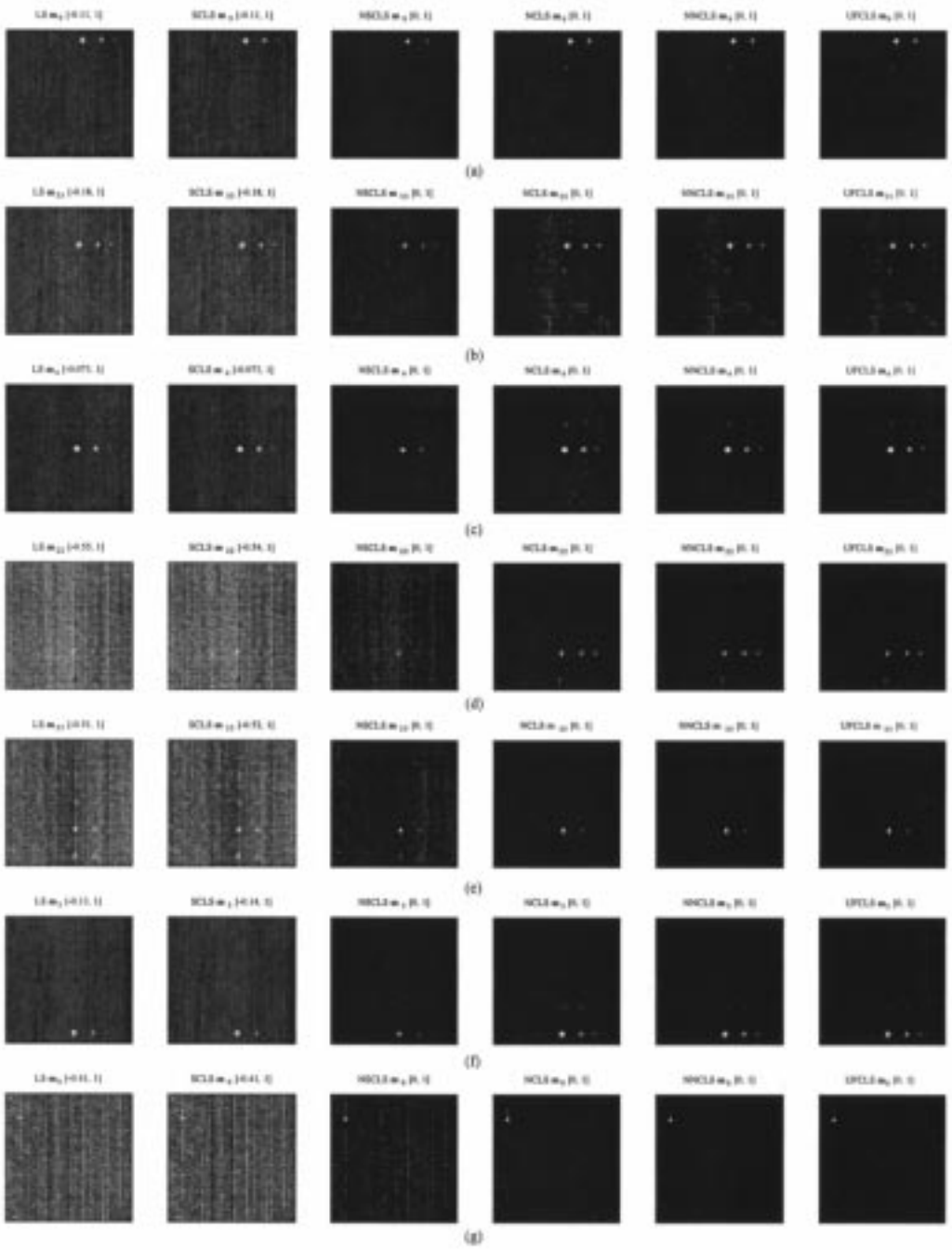

Fig. 16. Results of LS, SCLS, NSCLS, NNCLS, and UFCLS methods using endmembers generated by the UFCLS algorithm.

a white-masked pixel next to top black-masked pixel of panel p_{21}.

It should be noted that in this unsupervised case, the UFCLS algorithm actually detected the panels in row 4 in two separate images. This separation could have been avoided if the UFCLS algorithm was terminated at iteration 34 or 35. However, determining the most appropriate stopping threshold is generally difficult due to the lack of prior information. As we can see from these images, the NCLS, NNCLS and UFCLS methods performed the best and significantly better than the LS, SCLS and NSCLS methods. A similar anomaly detection to that shown in Fig. 8(d) was also observed in Fig. 16(g), where there was an unknown signature detected in the upper left corner of the tree line. Tables V and VI contain quantification results for the entire image and for the black and white-masked pixels respectively. As we can see from the quantification values in these two tables, the NCLS, NNCLS and UFCLS performed significantly better than the other methods.

This last experiment was able to show that the UFCLS method could effectively detect and quantify materials in an unknown image scene. However, since the UFCLS method was completely unsupervised, further analysis would be required to identify all the unknown materials. This can generally be done by calibrating the spectra of the extracted material signatures and comparing them against a reference database such as a spectral library for material quantification.

TABLE V
SUM OF QUANTIFICATION RESULTS OVER ALL IMAGE PIXELS FOR LS, SCLS, NSCLS, NCLS, NNSCLS, AND UFCLS METHODS USING MATERIAL SIGNATURES GENERATED BY THE UFCLS METHOD

	LS	SCLS	NSCLS	NCLS	NNCLS	UFCLS
$\mathbf{m}_9$	-49.2866	-53.4773	8.5554	9.0078	9.0037	9.5068
$\mathbf{m}_{33}$	22.6381	37.7144	34.2775	34.4859	34.7202	28.3764
$\mathbf{m}_4$	45.0890	45.0504	23.0562	22.9769	22.9950	24.9895
$\mathbf{m}_{22}$	186.1792	202.9720	109.4225	7.0436	6.9863	8.7071
$\mathbf{m}_{35}$	-135.5971	-143.8910	52.4539	3.2501	3.1987	6.5286
$\mathbf{m}_3$	7.5093	-1.95281	9.8006	8.8974	8.8122	8.4374

TABLE VI
SUM OF QUANTIFICATION RESULTS OVER ONLY BLACK AND WHITE-MASKED PIXELS FOR LS, SCLS, NSCLS, NCLS, NNSCLS, AND UFCLS METHODS USING MATERIAL SIGNATURES GENERATED BY THE UFCLS METHOD

	LS	SCLS	NSCLS	NCLS	NNCLS	FCLS
p_{11}	3.21	3.14	1.74	3.14	3.12	2.96
p_{12}	1.02	0.97	0.49	1.29	1.28	1.26
p_{13}	-0.23	-0.23	0.06	0.09	0.09	0.05
p_{21}	5.21	4.96	2.37	3.70	3.69	3.37
p_{22}	1.20	1.30	0.56	1.20	1.17	1.43
p_{23}	0.47	0.52	0.23	0.57	0.56	0.61
p_{31}	4.01	4.01	1.91	4.09	4.10	4.03
p_{32}	2.52	2.52	0.86	1.95	1.94	1.96
p_{33}	0.77	0.77	0.25	0.49	0.49	0.50
p_{41}	4.70 + - 0.97	4.79 + - 1.01	2.18 + 1.20	1.94 + 1.57	1.90 + 1.54	1.97 + 2.05
p_{42}	-0.19 + 2.82	0.12 + 2.66	0.38 + 0.90	1.42 + 0.33	1.41 + 0.33	1.47 + 0.35
p_{43}	0.81 + - 0.12	0.93 + - 0.18	0.29 + 0.08	0.54 + 0	0.53 + 0	0.60 + 0
p_{51}	4.51	4.54	2.14	3.85	3.81	3.69
p_{52}	1.51	1.51	0.50	1.85	1.84	1.79
p_{53}	0.28	0.19	0.09	0.47	0.46	0.45

VII. CONCLUSION

Unconstrained linear unmixing has been used for hyperspectral image classification for mathematical tractability. In this case, the solved abundance fractions of material signatures may be negative and their sum within an image pixel may not necessarily be one. As a consequence, such unconstrained solutions are generally not optimal in terms of material quantification. This paper presented an FCLS linear unmixing method. It is a least squares approach that simultaneously imposes two constraints, the ASC and the ANC, on the linear mixture model. Since there is no closed form solved for fully constrained linear mixing problems, an efficient algorithm is further developed to generate the desired optimal solutions. In implementing the FCLS method, a complete knowledge of material signatures is required. In order to relax this requirement, an unsupervised constrained LSE-based approach is also proposed to extend the FCLS method in an unsupervised fashion, so that all the desired material information can be obtained directly from an unknown image scene. Despite a slight degradation in quantification performance, this resulting unsupervised FCLS (UFCLS) method has a significant advantage that the FCLS does not have. That is, it can be used for finding and quantifying anomalies. This has been demonstrated by computer simulations and real hyperspectral image experiments. It was shown that the NCLS, NNCLS and FCLS methods performed significantly better than the LS, SCLS, and NSCLS methods as the number of material signatures in the signature matrix is increased or as the signatures of materials become more similar.

ACKNOWLEDGMENT

The authors would like to thank the Bechtel Nevada Corporation for their support and Dr. J. C. Harsanyi for providing the AVIRIS data.

REFERENCES

[1] R. A. Schowengerdt, *Remote Sensing: Models and Methods for Image Processing*, 2nd ed. New York: Academic, 1997, pp. 470–471.
[2] J. B. Adams and M. O. Smith, "Spectral mixture modeling: A new analysis of rock and soil types at the Viking lander 1 suite," *J. Geophys. Res.*, vol. 91, no. B8, pp. 8098–8112, July 10, 1986.
[3] J. B. Adams, M. O. Smith, and A. R. Gillespie, "Simple models for complex natural surfaces: A strategy for hyperspectral era of remote sensing," in *Proc. IEEE Int. Geoscience and Remote Sensing Symp. '89*, 1989, pp. 16–21.
[4] A. F. H. Goetz and J. W. Boardman, "Quantitative determination of imaging spectrometer specifications based on spectral mixing models," in *Proc. IEEE Int. Geoscience and Remote Sensing Symposium '89*, 1989, pp. 1036–1039.
[5] A. R. Gillespie, M. O. Smith, J. B. Adams, S. C. Willis, A. F. Fischer, III, and D. E. Sabol, "Interpretation of residual images: Spectral mixture analysis of AVIRIS images," in *Proc. 2nd AVIRIS Workshop*, Owens Valley, CA, 1990, pp. 243–270.
[6] D. E. Sabol, J. B. Adams, and M. O. Smith, "Quantitative sub-pixel spectral detection of targets in multispectral images," *J. Geophys. Res.*, vol. 97, pp. 2659–2672, 1992.
[7] J. B. Adams, M. O. Smith, and A. R. Gillespie, "Image spectroscopy: Interpretation based on spectral mixture analysis," in *Remote Geochemical Analysis: Elemental and Mineralogical Composition*, C. M. Pieters and P. A. Englert, Eds. Cambridge, U.K.: Cambridge Univ. Press, 1993, pp. 145–166.
[8] M. O. Smith, J. B. Adams, and D. E. Sabol, "Spectral mixture analysis—New strategies for the analysis of multispectral data," in *Image Spectroscopy—A Tool for Environmental Observations*, J. Hill and J. Mergier, Eds. Brussels, Belgium: ECSC, EEC, EAEC, 1994, pp. 125–143.
[9] M. O. Smith, D. A. Roberts, J. Hill, W. Mehl, B. Hosgood, J. Verdebout, G. Schmuck, C. Koechler, and J. B. Adams, "A new approach to quantifying abundances of materials in multispectral images," in *Proc. IEEE Int. Geoscience and Remote Sensing Symposium '94*, Pasadena, CA, Aug. 1994, pp. 2372–2374.
[10] S. Tompkins, J. F. Mustard, C. M. Pieters, and D. W. Forsyth, "Optimization of endmembers for spectral mixture analysis," *Remote Sens. Environ.*, vol. 59, pp. 472–489, 1997.
[11] R. B. Singer and T. B. McCord, "Mars: Large scale mixing of bright and dark surface materials and implications for analysis of spectral reflectance," in *Proc. 10th Lunar Planetary Science Conf.*, 1979, pp. 1835–1848.
[12] B. Hapke, "Bidirection reflectance spectrocopy. I. Theory," *J. Geophys. Res.*, vol. 86, pp. 3039–3054, 1981.
[13] P. Johnson, M. Smith, S. Taylor-George, and J. Adams, "A semiempirical method for analysis of the reflectance spectra of binary mineral mixtures," *J. Geophys. Res.*, vol. 88, pp. 3557–3561, 1983.
[14] R. O. Duda and P. E. Hart, *Pattern Classification and Scene Analysis*. New York: Wiley, 1973.
[15] J. T. Tou and R. C. Gonzalez, *Pattern Recognition Principles*. Reading, MA: Addison-Wesley, 1974.
[16] R. Schalkoff, *Pattern Recognition: Statistical, Structure and Neural Network*. New York: Wiley, 1992.
[17] J. W. Boardman, "Inversion of imaging spectrometry data using singular value decomposition," in *Proc. IEEE Geoscience and Remote Sensing Symp.* , 1989, pp. 2069–2072.
[18] J. J. Settle, "On the relationship between spectral unmixing and subspace projection," *IEEE Trans. Geosci. Remote Sensing*, vol. 34, pp. 1045–1046, July 1996.
[19] C.-I Chang, "Further results on relationship between spectral unmixing and subspace projection," *IEEE Trans. Geosci. Remote Sensing*, vol. 36, pp. 1030–1032, May 1998.
[20] Y. E. Shimabukuro and J. A. Smith, "The least-squares mixing models to generate fraction images derived from remote sensing multispectral data," *IEEE Trans. Geosci. Remote Sensing*, vol. 29, pp. 16–20, Jan. 1991.

[21] C.-I Chang, X. Zhao, M. L. G. Althouse, and J.-J. Pan, "Least squares subspace projection approach to mixed pixel classification in hyperspectral images," *IEEE Trans. Geosci. Remote Sensing*, vol. 36, pp. 898–912, May 1998.
[22] J. C. Harsanyi and C.-I Chang, "Hyperspectral image classification and dimensionality reduction: An orthogonal subspace projection," *IEEE Trans. Geosci. Remote Sensing*, vol. 32, pp. 779–785, July 1994.
[23] T. M. Tu, C.-H. Chen, and C.-I Chang, "A least squares orthogonal subspace projection approach to desired signature extraction and detection," *IEEE Trans. Geosci. Remote Sensing*, vol. 35, pp. 127–139, Jan. 1997.
[24] C.-I Chang, T. L. E. Sun, and M. L. G. Althouse, "An unsupervised interference rejection approach to target detection and classification for hyperspectral imagery," *Opt. Eng.*, vol. 37, pp. 735–743, Mar. 1998.
[25] J. Boardman, "Inversion of high spectral resolution data," *Proc. SPIE*, vol. 1298, pp. 222–233, 1990.
[26] Y. E. Shimabukuro, "Shade images derived from linear mixing models of multispectral measurements of forested areas," Ph.D. dissertation, Dept. Forest Wood Sci., Colorado State Univ., Fort Collins, 1987.
[27] J. J. Settle and N. A. Drake, "Linear mixing and estimation of ground cover proportions," *Int. J. Remote Sensing*, vol. 14, no. 6, pp. 1159–1177, 1993.
[28] E. A. Ashton and A. Schaum, "Algorithms for the detection of sub-pixel targets in multispectral imagery," *Photogramm. Eng. Remote Sensing*, pp. 723–731, July 1998.
[29] L. L. Scharf, *Statistical Signal Processing*: Addison-Wesley, 1991.
[30] C.-I Chang and D. Heinz, "Subpixel spectral detection for remotely sensed images," *IEEE Trans. Geosci. Remote Sensing*, vol. 38, pp. 1144–1159, May 2000.
[31] D. Heinz, C.-I Chang, and M. L. G. Althouse, "Fully constrained least squares-based linear unmixing," in *Int. Geoscience and Remote Sensing Symp. '99*, Hamburg, Germany, June 28–July 2 1999, pp. 1401–1403.
[32] K. H. Haskell and R. J. Hanson, "An algorithm for linear least squares problems with equality and nononegativity constraints generalized," *Math. Prog.*, vol. 21, pp. 98–118, 1981.
[33] C. L. Lawson and R. J. Hanson, *Solving Least Squares Problems*. Philadelphia, PA: SIAM, 1995, vol. 15.
[34] H. Ren and C.-I Chang, "A computer-aided detection and classification method for concealed targets in hyperspectral imagery," in *Int. Symp. Geoscience and Remote Sensing '98*, Seattle, WA, July 5–10, 1998.
[35] ——, "A generalized orthogonal subspace projection approach to unsupervised multispectral image classification," *IEEE Trans. Geosci. Remote Sensing*, vol. 38, pp. 2515–2528, Nov. 2000.
[36] D. Heinz and C.-I Chang, "Constraint least squares linear spectral mixture methods for material abundance estimation, discrimination, detection, classification, identification, recognition and quantification, data compression and noise estimation in hyperspectral and multispectral imagery," Disclosure of Invention, Feb. 14, 2000.
[37] C.-I Chang, "Spectral information divergence for hyperspectral image analysis," in *Int. Geoscience and Remote Sensing Symp. '99*, Hamburg, Germany, June 28–July 2 1999, pp. 509–511.
[38] ——, "An information theoretic-based approach to spectral variability, similarity and discriminability for hyperspectral image analysis," *IEEE Trans. Inform. Theory*, pp. 1927–1932, Aug. 2000.
[39] C. Brumbley, "Kalman filtering and subspace projection approaches to multispectral and hyperspectral image classification," Ph.D. dissertation, Dept. Comp. Sci. Elect. Eng., Univ. Maryland, Baltimore County, May 1998.

Daniel C. Heinz (S'92) received the B.S. and M.E.S. degrees in electrical engineering from the State University of New York, Buffalo, and Loyola College, Baltimore, MD, in 1991 and 1994, respectively. He is currently pursuing the Ph.D. degree in the Department of Computer Science and Electrical Engineering, University of Maryland, Baltimore County (UMBC), Baltimore.

He worked on a chemical detector project at the United States Army Chemical and Biological Defense Command, Aberdeen Proving Ground, Aberdeen, MD, from 1991 to 1996. From 1996 to 1997, he worked on video teleconferencing at Tracor Applied Sciences, Inc., California, MD. From 1998 to 1999, he worked as a Teaching and Research Assistant with UMBC. Currently, he is an Instructor at UMBC. His research interests include digital signal processing, image processing, and remote sensing.

Mr. Heinz is a member of SPIE and Phi Kappa Phi.

Chein-I Chang (S'81–M'87–SM'92) received the B.S. degree from Soochow University, Taipei, Taiwan, in 1973, the M.S. degree from the Institute of Mathematics, National Tsing Hua University, Hsinchu, Taiwan, 1975, and the M.A. degree from the State University of New York, Stony Brook, in 1977, all in mathematics. He also received the M.S. and M.S.E.E. degrees from the University of Illinois, Urbana, in 1982, and the Ph.D. degree in electrical engineering from the University of Maryland, College Park, in 1987.

He has been with the University of Maryland-Baltimore County (UMBC), Baltimore, as a Visiting Assistant Professor from January 1987 to August 1987, Assistant Professor from 1987 to 1993, and has been an Associate Professor in the Department of Computer Science since 1993. He was a Visiting Research Specialist in the Institute of Information Engineering, National Cheng Kung University, Tainan, Taiwan, from 1994 to 1995. He has a patent on automatic pattern recognition and several pending patents on image processing techniques for hyperspectral imaging and detection of microcalcifications. He is currently on the editorial board of *Journal of High Speed Networks* and is the Guest Editor of a special issue of that journal on telemedicine and applications. His research interests include automatic target recognition, multispectral/hyperspectral image processing, medical imaging, information theory and coding, signal detection and estimation, and neural networks.

Dr. Chang is a member of SPIE, INNS, Phi Kappa Phi, and Eta Kappa Nu.